

Master's Programme in Building Technology

Developing a novel technique for testing glass strength

Mohamed Sherif

Master's Thesis
2025

Copyright ©2025 Mohamed Sherif

Author Mohamed Sherif

Title of thesis Developing a novel technique for testing glass strength

Programme Building Technology

Thesis supervisor Sergei Khakalo, Asst. Prof.

Thesis advisors Janne Heiskari, D.Sc.; Pauli Lehto, D.Sc.

Date 29.09.2025

Number of pages 72

Language English

Abstract

The use of glass in structural applications has become more and more prevalent, with applications like modern cruise ships incorporating large glass façades into their architecture. With this trend ongoing, the concept of structural optimization is naturally extended to reach glass elements, as part of a global shift towards light-weight, more sustainable design. The foundation of an optimized glass structural element is an efficient method for strength determination. Glass is a brittle material; that is, its strength is primarily driven by the flaws existing in its surface rather than intrinsic bond strength between atoms. This makes characterizing its strength a challenging task. For this reason, glass strength should be tested so that a uniform biaxial stress field is created within the test area to eliminate the influence of the orientation of surface flaws, as flaws are most critical when they are normal to the direction of the maximum stress. The four-point-bending test (4pb) and the coaxial double ring (CDR) test are two of the most common standardised testing methods for glass strength. However, these tests do not present efficient methods for determining glass strength, as the former includes glass edges, where flaws are more critical, within the region of maximum stress, while the latter only considers small specimens. For large specimens that undergo large deflections where the effect of geometric nonlinearity is significant, the standardized approach for the CDR test not only becomes overly sophisticated, but it also fails to maintain an equibiaxial stress state. This thesis aims to propose a novel technique for testing glass strength, utilizing the CDR method, that is simpler and more efficient than the current common testing methods. 21 identical fully tempered glass specimens of dimensions 1000×1000×6 mm were tested using the proposed technique, utilizing tools like Digital Image Correlation (DIC) and strain gauges for data acquisition. The results showed that the proposed test setup is capable of reproducing the same loading and boundary conditions for the majority of the tested specimens, while maintaining a somewhat uniform stress field under large deflections. Overall, the proposed test setup showed efficacy and potentially presents a simpler and reliable alternative to the standardised testing methods currently in use.

Keywords: Tempered glass; Glass strength testing; Digital image correlation (DIC); Coaxial double ring test.

Preface and acknowledgements

The work in this thesis has been performed at the Department of Mechanical Engineering at Aalto University as part of CaNelis Project. The financial support provided by the project is gratefully acknowledged. I would like to thank my supervisors, Pauli Lehto, Janne Heiskari, and Sergei Khakalo, for their support throughout my journey of completing this work.

Table of contents

1	Introduction	7
1.1	General background.....	7
1.2	Problem statement.....	8
1.3	Scope and objectives	9
1.4	Research methodology.....	10
1.5	Outline and structure.....	11
2	Glass: composition, production, and application	13
2.1	Chemical composition of glass	13
2.2	Production technology and processing of glass.....	15
2.3	Applications of glass	19
3	Strength of glass	22
3.1	Theoretical versus practical strength	22
3.2	Fracture mechanics.....	23
3.3	Statistical interpretations of glass strength.....	26
3.4	Testing methods of glass strength	30
4	Experimental program	34
4.1	Test setup	34
4.2	Test specimens and preparations	36
4.3	Pressure control system.....	37
4.4	Data acquisition	38
4.5	Locating the failure origin	40
4.6	Error minimization measures.....	42
4.7	Challenges and adaptations in the experimental setup	43
5	Results	47
5.1	Time history response.....	48
5.2	Load-deflection relationship.....	48
5.3	Strain gauges results	50
5.4	DIC results	51
6	Discussion and conclusions	58
6.1	Main findings	58

6.2	Discussion of results	59
6.3	Conclusions and future work.....	60
	References.....	62
	Appendix A.....	66
	Appendix B.....	78

1 Introduction

1.1 General background

Glass has established itself as a cornerstone material across various industries, including construction, transportation, and maritime. While it is mostly used for windows and doors, there are also remarkable efforts to use glass as load-bearing structural elements, such as beams and floors. This strong appeal for glass comes not only from its high aesthetic value and transparency, but also from its impressive mechanical properties and durability. For example, using glass as a structural material in buildings can offer many advantages, such as reducing the need for artificial lighting due to its ability to allow natural light to pass through it, promoting energy efficiency, and improving well-being. Also, glass can be used in a great variety of architectural and industrial applications, making it a versatile option for architects and engineers.

The term “glass” is comprehensive, and it encompasses a varied range of types and forms, each with its distinct properties influenced by its composition and manufacturing method. At its core, glass can be defined as any amorphous solid material that, when heated well above its melting point and then cooled down from a liquid to a solid state, does not form a repeating and regular atomic structure (crystallization) but transitions gradually to a solid state without having a uniform atomic pattern. This characteristic is called glass transformation behavior, and it is what fundamentally distinguishes glass from crystalline materials (e.g., most metals) [1].

With this broad definition, we can trace the use of glass as early as ancient times, when humans used naturally occurring glass to make tools and weapons. On the other hand, the production of artificial man-made glass can be dated back to 7000 BC in Mesopotamia [2]. Since then, glass has been used extensively in various industries: from the making of bottles and jars to the windows of buildings, ships, and aircraft.

As a material with this wide range of applications, it is only natural that glass has been a substantial research topic over the past years. Particularly, the mechanical properties of glass (strength, brittleness, elasticity, etc.) have been extensively researched. Glass is a brittle material, meaning it tends to suddenly fracture under stress rather than exhibiting plastic deformation. Also, when glass breaks, it shatters into sharp pieces that can penetrate objects and cause injuries. This behavior can be dangerous, and that is the reason for the different kinds of manufacturing processes that have been developed to enhance the material’s safety performance. One of these processes is tempering, which is done by heating the material well above its transformation temperature and then rapidly cooling it through air jets. When

broken, tempered glass shatters into small, rounded pieces instead of sharp shards, which significantly improves the safety aspect of the material.

Moreover, tempered glass is about four times stronger than its untempered counterpart [1,3], paving the way for its utilization in different structural applications. However, because glass strength is heavily dependent on the type and distribution of surface flaws and imperfections, there is a significant variability in its value, ranging from 20 MPa to 160 MPa [3,4]. As a result, a very conservative safety factor is usually applied in practical applications [5,6], leading to an unnecessary use of material, which adds to the weight of the structure. Thus, a more solid understanding of glass strength will not only be of an economical value, but it will also promote sustainability through a more optimized use of materials and reducing waste.

1.2 Problem statement

Glass can be considered as an isotropic homogenous material with a linear-elastic behaviour. It is also a brittle material that has a very high compressive strength compared to its tensile strength. The brittleness of glass manifests itself as a sudden fracture whenever it is subjected to a tensile stress that exceeds its fracture strength. The fracture strength of manufactured glass is generally orders of magnitude lower than the theoretical strength calculated for it; this is because of the flaws that are randomly distributed across its surface. Internal stresses get concentrated at the locations of these flaws, creating a localized stress that exceeds the theoretical strength [1], causing the material to break suddenly. Surface flaws in glass can take any shape, but they are usually semi-circular, and their orientation is random [7]. Surface flaws are most critical when they are perpendicular to the direction of the maximum principal stress. That makes the task of predicting the fracture strength of glass very challenging. Consequently, testing of glass strength should be performed in a way that rules out potential sources of uncertainty and reflects the real loading conditions of glass in practical applications.

The Coaxial Double Ring (CDR) is a standard testing method of glass strength where a specimen is placed between two concentric rings with different dimensions, and the load is applied through the inner ring. This method can produce a biaxial flexural stress within the loaded area that is uniform in all directions, thus eliminating the influence of the orientation of the surface flaws on the results. This ideal stress condition is, however, achievable only in the case of small deflection, according to the European standard EN 1288-1 [8]. So, in case of specimens with a large test area that are likely to exhibit larger deformations, the EN 1288-1 recommends using an additional overpressure that is adjusted with respect to the applied force. This overpressure is intended to compensate for the effects of localized stresses that are formed along the contact area of the loading ring,

maintaining an equibiaxial stress condition. This combination of the ring load and overpressure, however, is problematic because not only is it overly sophisticated and makes performing the test more difficult [9,10], but it also fails to adequately compensate for the geometric nonlinear effects and, in turn, fails to create an equibiaxial stress state [11,12]. Moreover, even with the assumption that an equibiaxial stress is achievable using additional overpressure, the large deformations and, in turn, geometric nonlinear behavior are still present. Yet, the EN 1288 standard relies on using a linear elastic solution under the assumption of small deflections (simple bending theory) to evaluate the flexural stress, even though this approach does not account for the in-plane tensile stresses that are associated with the geometrically nonlinear behavior of plates [13]. This approach, consequently, calculates stresses that are higher than the actual stresses, understating the true strength of large glass panes. It should be noted that using the simple bending theory allows for a quick and convenient way to calculate glass strength for structural design purposes. This, however, comes at the cost of a suboptimal design, and this trade-off can be too expensive in applications where glass is used extensively (e.g., modern cruise ships).

It is worth mentioning that the majority of glass used in buildings as well as ships has a large surface area and a small thickness, meaning that they develop a geometrically nonlinear behavior. Accordingly, accounting for geometric nonlinearities has significant importance in designing more efficient and sustainable glass structural elements. For this reason, a favored testing method of glass strength should promote the development of geometric nonlinear behavior, and proper calculation methods should then be used to account for it.

In addition, to the knowledge of the author, there have been no experiments made on fully tempered glass panes with a large surface area using the CDR testing method. The lack of research on this subject matter leaves the behavior of tempered glass not fully understood, which reflects on the design of practical applications involving it. Accordingly, more research is needed in this field to build a more solid understanding of tempered glass strength.

1.3 Scope and objectives

The main aim of this study is to develop and propose a novel technique for testing glass strength that is simpler and more efficient than the current standard testing methods. The proposed technique is a novel implementation of the CDR testing method. Biaxial strength testing is selected as a preferred testing method over uniaxial testing because it rules out the influence of the direction of surface flaws, as well as being more reflective of real loading scenarios. As well, studying the strength of annealed glass lies outside the scope of this research, since tempered glass is more commonly used in

structural contexts. Towards the aim of this research, the focal objectives to be achieved are:

- To employ the geometric nonlinear behaviour of glass favorably to put forward a more representative picture of the strength of glass used in practice.
- To provide new and valuable information on testing tempered glass panes with a large test area, in particular, and the strength of brittle materials in general.
- To refine and optimize a new technique for testing glass strength that is mainly designed for, but not limited to, glass panes with large surface area.
- To propose a novel technique for the CDR method that is simpler and more efficient than the current standard testing methods.

1.4 Research methodology

To achieve the objectives of this research, an experimental program is conducted using the CDR test method with a novel technique. A total of 21 large fully tempered glass panes with nominal dimensions $1000 \times 1000 \times 6$ mm are be tested with a uniform pressure applied through water. The dimensions of the test specimens will allow for having a large surface area under biaxial flexural stress, which will increase the probability of having a dominant crack present, thus providing a representative picture of glass defectiveness. Also, large test specimens will allow for the development of geometric nonlinearity. As the testing of the specimens progresses, refinements to the test setup will be implemented as needed to improve functionality and achieve consistency in results.

Displacement and pressure sensors are be used to record the central deflection and the water pressure during testing. In addition, Digital Image Correlation (DIC) is utilized to record the strain and displacement within the whole test area. This will allow for a comprehensive representation of the glass behaviour. However, DIC data require a large digital storage capacity, which makes it challenging to use for all the tested specimens, and therefore it is only used for a small subset of tests. As well, strain gauges are be utilized in a limited number of tests to measure the in-plane strain in selected locations. The strain gauges' results will be examined alongside the results recorded by the DIC for validation and comparison. Given the linear elastic behaviour of glass, the in-plane principal stresses can be evaluated through simple calculations using the measured strain. In proper testing conditions, the fracture should initiate inside the loaded area. Therefore, specimens with a fracture initiated outside or along the periphery of the loading ring will constitute invalid tests.

1.5 Outline and structure

This thesis consists of five chapters plus the introductory chapter 1. The two chapters following the introduction serve as a general background and a review of the relevant literature. The fourth chapter introduces the experimental program, the fifth chapter presents the relevant results and findings, and the last chapter is dedicated to a discussion and the main conclusions of the work. A more elaborate description of the thesis outline is presented below. Additionally, a graphical overview of the thesis is shown in Figure 1.1.

Chapter 2 – This chapter starts with the chemical composition of glass. It then goes over the most relevant production techniques of glass and finally ends with a review of the most common applications of glass.

Chapter 3 – This chapter discusses the strength of glass. It aims to provide a theoretical background on the underlying mechanics of glass elements. It also goes over the statistical nature of glass strength and the relevant statistical methods used to model it. Lastly, this chapter provides an overview of the relevant testing methods for glass strength.

Chapter 4 – This chapter describes the proposed testing technique. It explains the test setup, the test specimens, the loading method, and the instrumentation used for acquiring the data. This chapter also discusses the sources of random errors, and the techniques used to eliminate systematic errors. Moreover, it goes over the most important modifications incorporated into the test setup throughout the testing process.

Chapter 5 – This chapter presents the relevant results. Time history response for load and deflection is presented. The load vs deflection relationship for all the tested specimens is shown. The strain results obtained from strain gauges, along with the corresponding stress calculated from them, are shown. Additionally, principal strain and principal stress data obtained through digital image correlation are presented.

Chapter 6 – This chapter provides a summary of the main results and findings. A brief discussion is included, as well as the main conclusions of the work. This chapter closes the thesis with recommendations for future research.

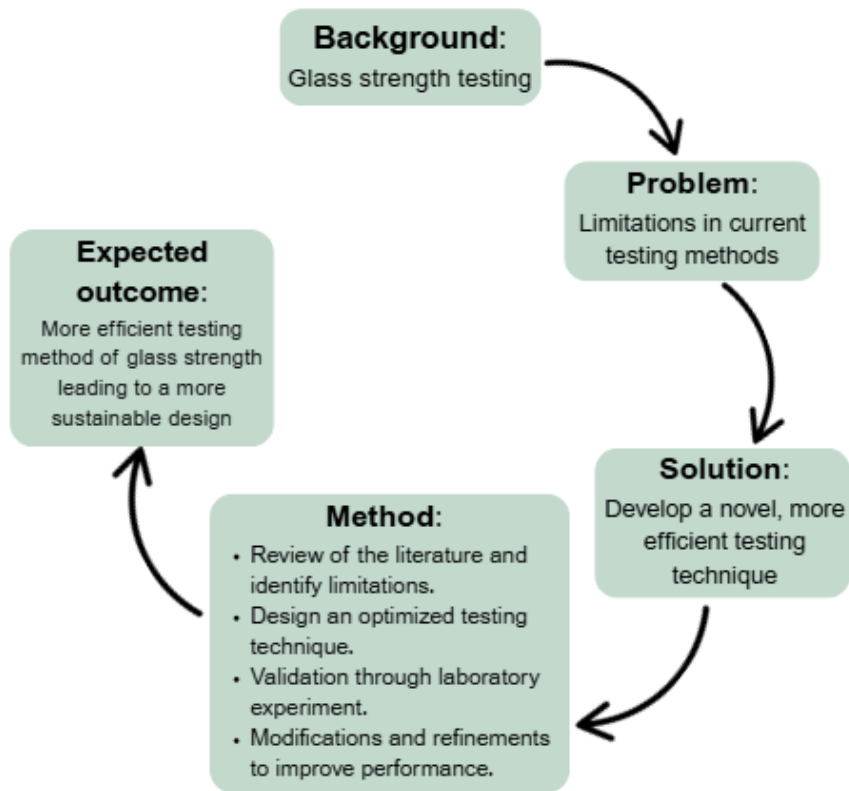


Figure 1.1 Graphical overview of the thesis.

2 Glass: composition, production, and application

2.1 Chemical composition of glass

Glass is any amorphous solid lacking long-range order of atomic arrangement that exhibits glass transition behaviour. That is, when a material is heated above the glass transition temperature (the temperature at which amorphous materials transform from a solid state to a viscous state), then cooled below this temperature, a non-crystalline solid is formed without any long-range, periodic atomic arrangement (see Figure 2.1). Virtually, any material can be formed into glass, even metals and polymers [1]. Glass can be organic, such as obsidian and fulgurite, which were used by humans since as early as 5000 BC. However, most of the commercial glass in use currently is artificial. There are various types of man-made glass depending on its chemical composition.

Borosilicate glass, vitreous silica, and soda-lime-silica glass are the most common commercially available types of glass. Borosilicate glass is characterized by having improved thermal shock resistance, electrical resistance, and chemical durability, and hence, they are commonly used in cookware, laboratory equipment, and optical instruments. Vitreous silica glass is mainly made from silicon dioxide (SiO_2). It has an extremely low coefficient of thermal expansion as well as a good optical transparency, which makes it suitable for applications such as optical fibres for telecommunications, optical lenses and prisms, and laboratory glassware.

Soda-lime-silica glass, on the other hand, is by far the most widely available commercial glass. It is the most commonly used glass for building fenestration, ship windows, and other structural applications. Therefore, soda-lime-silica glass will be the focus of this research. The main ingredient of soda-lime-silica glass is silica (silicon dioxide). Soda (Sodium oxide; Na_2O) is added to silica to lower its glass transition temperature, making it more workable. Adding soda in massive amounts, however, leads to an inadequate chemical durability. On that account, a portion of soda is replaced by lime (calcium oxide; CaO) to maintain an acceptable level of chemical durability while reasonably reducing the glass transition temperature [1, 14]. In addition to silica, soda, and lime, there are other elements such as magnesium oxide (MgO), ferric oxide (Fe_2O_3), and aluminum oxide that can be added to improve durability [14].

At an atomic level, the silicon atom (Si), the primary element of the composition of soda-lime-silica glass, bonds with four oxygen atoms (O) with the Si atom being in the center, forming an oxygen tetrahedron. Each oxygen tetrahedra pair is connected through the corners to create the atomic structure of SiO_2 . Silicon dioxide network can have a long-term order with a repeating

pattern, allowing for the prediction of the position of any atom in the network, which characterizes it as a crystal (Figure 2.1a). Or it can be found in a glassy form, which lacks any long-term order, making the prediction of the atomic arrangement within the network no longer possible (Figure 2.1b). The addition of sodium oxide (Na_2O) modifies the structure in a way that decreases the viscosity of the glass melt and thus lowers the glass transition temperature from as high as 1700°C to around 790°C [15]. The Na_2 -modified network is shown in Figure 2.1c. Calcium oxide is, then, added to the structure so that the alkaline Ca^{+2} ions impede the easy migration of the alkali Na^+ ions of Na_2 , resulting in an improvement of the glass chemical durability [15].

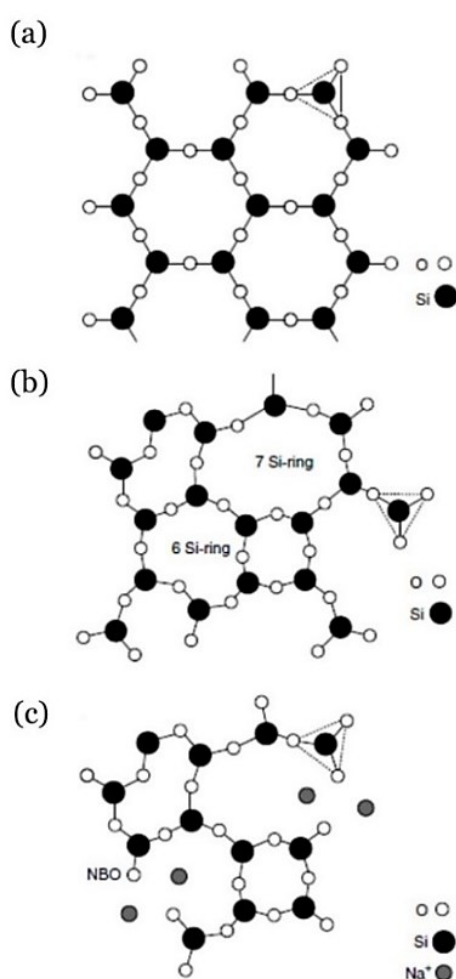


Figure 2.1 2D atomic network of silicon dioxide (SiO_2): (a) crystalline form of SiO_2 where long-term order exists; (b) glassy form of SiO_2 that lacks any long-term order; (c) Na_2 -modified glassy form of SiO_2 .

2.2 Production technology and processing of glass

Glass production involves four principal operations: batching, melting, fining, and forming. Batching is the first step of glass production; it is done by selecting and mixing the raw materials based on characteristics such as purity and particle size. Batching is followed by the melting of the well-mixed ingredients using either combustion or an electrical furnace. The next step is fining, which helps in homogenising the melt and removing air bubbles. It can be achieved through adding fining agents, such as arsenic and antimony, to the mix during batching. The fining phase is critical as it can affect glass forming. The final phase in glass production is glass forming. Numerous forming techniques have been developed to serve different applications.

Blow-and-Blow and Press-and-Blow processes are two commonly used processes to make glass bottles and containers. They involve shaping the molten glass through moulds and blowing. Another common forming process is the Fusion Draw process, which is especially effective in making very thin glass that is used in applications like touch screens and display panels. The most common glass-forming process, however, is the float process. It accounts for the vast majority of the flat glass produced, and therefore it will be discussed in detail in this section. Moreover, glass can be subjected to further processing to improve its mechanical properties. Aside from the basic annealing process, thermal tempering, which includes heat-strengthened and fully tempered glass, and chemical tempering, are the most common methods to process glass; these methods will be discussed in this section with an emphasis on fully tempered glass, since it is used in the experiment conducted in this research.

Being responsible for around 90% of the overall flat glass production, the float process has been the most widely adopted technique for glass forming since its inception in the 1950s. Figure 2.2 summarizes the main stages of the float process. As it is implied by the name, the molten glass is poured to float on top of a bath of molten tin after the batch is melted in a furnace at a temperature of 1500°C. Due to its extensive temperature range in the liquid state, as well as its low density that allows glass to float on top of it, tin makes the perfect material for this application. The entering temperature of the molten

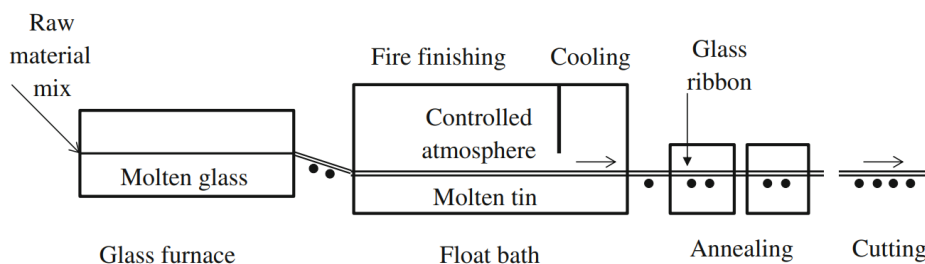


Figure 2.2 The float process [16].

glass to the tin bath is 1100°C; the glass melt exists in the bath at 600°C as a solidified ribbon [14]. The glass then passes on steel rollers that are water-cooled to control its thickness: the higher the rotation speed of the rollers, the thinner the glass sheet (see Figure 2.3). Glass sheets made through the float process can be as thin as 2 mm. In case a lower thickness is needed, other forming techniques are preferred (e.g., Fusion Draw process) [15]. After the desired thickness is achieved, the glass sheet enters a long oven called the lehr to impose a controlled slow cooling process from 600°C to room temperature. This phase is called annealing, and it is crucial to prevent excessive residual stresses from developing within the glass due to nonuniform cooling. Glass sheets are inspected, and those with visible flaws are discarded to be fed into the furnace again. As a final stage, glass sheets are cut into a standard size and then transferred to the storage section. This process proved to be superior to all other flat glassmaking techniques as it offers a cost-effective way for producing flat glass with an excellent optical quality without the need for any further processing. Accordingly, it is used to produce most of the flat glass worldwide. Glass produced through this process is called float glass, and it can be subjected to further processing, such as tempering, to alter its properties and increase its strength.



Figure 2.3 Thickness control of glass ribbon through rotating rollers [15].

The term tempering is generally used to indicate the strengthening of glass. Thermal tempering is achieved by rapidly cooling the glass through air jets after reaching its transition temperature to induce compression stresses into the surface and tensile stresses into the interior part, forming a parabolic stress profile shown in Figure 2.4. The compressive zone is about one-fifth of the glass thickness (h) from each side [14]. Since glass has a much higher compressive strength than tensile strength, this residual stress at the surface is considered favourable as it counteracts tensile stresses induced by loading

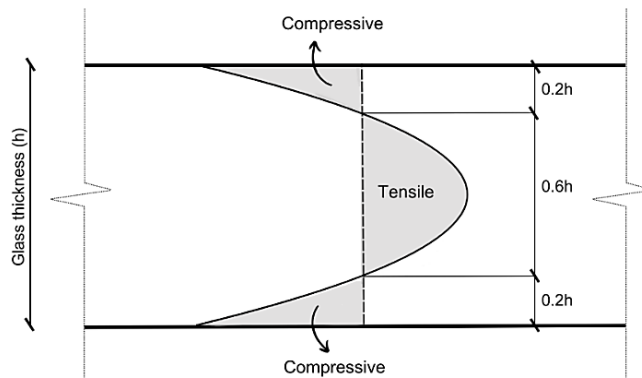


Figure 2.4 Stress profile of thermally tempered glass.

events such as wind pressure or wave loading in the case of ship windows. Figure 2.5 shows the main principle of glass tempering, illustrated by [17]. Also, the stored elastic energy within the glass makes it shatter into numerous small, rounded pieces instead of large pieces with sharp edges (see Figure 2.7); this significantly improves the safety aspect of the material. Float glass that is already formed can be tempered by heating the glass again near its transition temperature and then performing the thermal tempering process on it. Any cutting or modification in shape should, however, happen before tempering; otherwise, the pre-stress system will be disturbed.

It follows that determining the residual compressive stresses due to tempering is crucial for a controlled and more efficient production of tempered glass. Several mathematical models were developed for precisely that purpose. Starting with the freezing theory proposed in the 1920s [18], which assumes that the stresses are fixed at the transition temperature and does not account for the stress relaxation resulting from the viscoelastic behaviour of glass. This was addressed later by the viscoelastic theory (described in [15]).

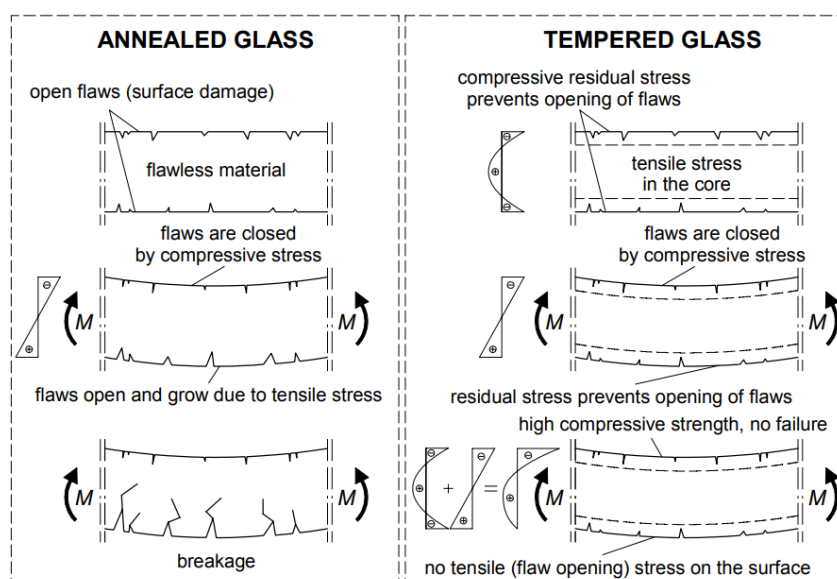


Figure 2.5 Working mechanism of tempered glass [17].

This theory, however, produced results that were not representative of experiments. This is because, along with viscoelastic relaxation, structural relaxation has to be accounted for as well. This was first addressed by Acloque in 1951, proposing a model accounting for both states of relaxation [19]. Finite Element Method (FEM) software can now be used to accurately predict the tempering-induced stresses in glass [20]. Typically, the residual compressive stress at the surface ranges between 80 MPa and 150 MPa for fully tempered glass [3,15].

Chemical tempering, also known as ion-exchange strengthening, can produce a surface compression up to four times that produced through thermal tempering (300-400 MPa) [21,22]; the values used in practical design, however, are considerably smaller than that. Since the process of chemical tempering is much more expensive compared to thermal tempering, it is only used in applications where exceptional safety levels are required (e.g., aeroplanes, high-speed train windshields, and armour). The tempering is achieved by the immersion of glass in a molten salt bath containing alkali ions larger than those present in the glass. Ionic diffusion then takes place between the alkali ions in the bath and the smaller ions in the glass. The existence of the larger ions that are squeezed into the glass surface creates a local strain which, in turn, produces a compressive stress in the glass surface [7,23]. Chemical tempering produces a stress profile, illustrated in Figure 2.6, that is very different from that shown in Figure 2.4, where the depth of the compression zone is only 30-40 μm and a very large tensile zone is much closer to the surface [7].

Heat-strengthened glass is considered partially tempered, as the process of producing it is similar to that of tempered glass but with a slower cooling rate. Heat-strengthening generates a lower surface compressive stress compared to fully tempered glass, and it is, therefore, weaker [15]. The stress profile in heat-strengthened glass is similar to that in Figure 2.4. When broken, heat-strengthened glass produces a fracture pattern that is intermediate between the patterns created by annealed and fully tempered glass. That is, it produces a larger number of pieces that are smaller in size than those produced by annealed glass, but much larger and sharper compared to tempered glass. Figure 2.7 shows a comparison between the fracture patterns associated with the three types of glass.

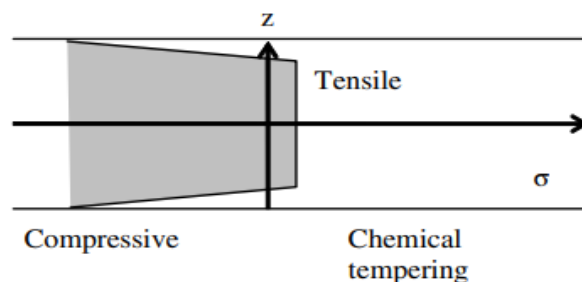


Figure 2.6 Residual stress profile from chemical tempering [15].

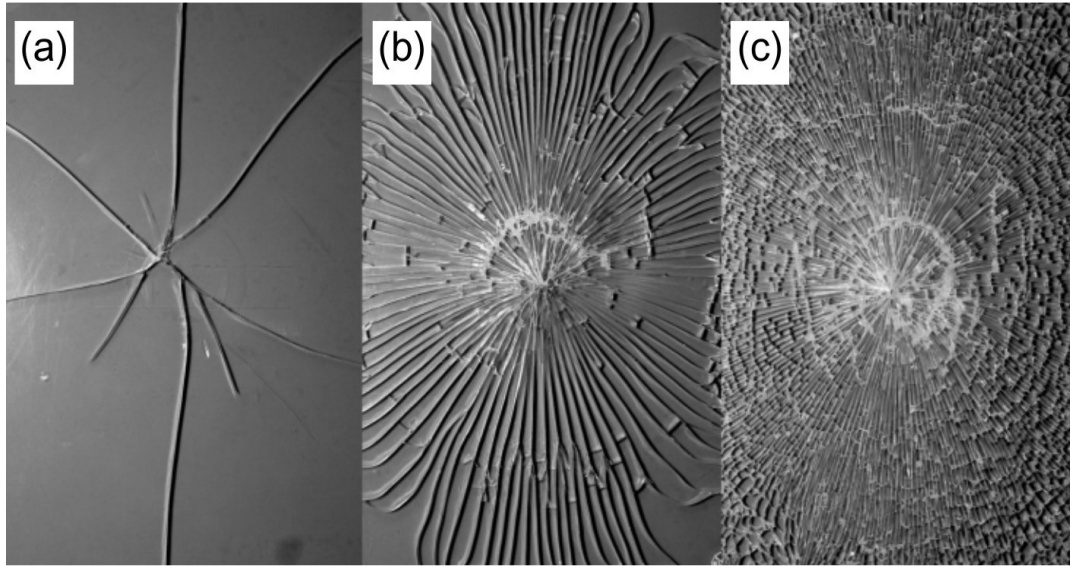


Figure 2.7 Fracture pattern of different glass types: (a) annealed glass; (b) heat-strengthened glass; (c) fully tempered glass [17].

2.3 Applications of glass

Glass has been used in various applications across multiple industries. Its optical properties, visual appeal, and mechanical properties make it suitable for applications, such as containers, building glazing, ship and aircraft windows, display and touch screens, and most recently as a load-bearing structural element in buildings (e.g., columns, beams, slabs). The applications of glass in the current day are numerous, to the point that it is virtually impossible to navigate simple daily activities without noticing it. The most relevant applications to this work (i.e., applications of a structural nature) will be reviewed in this section.

Due to its transparency, thermal performance, and high aesthetic value, glass has been a favoured material for architects in recent decades. Its transparency allows it to create a continuum of space between the indoor and outdoor. The use of glass in architecture started with the Romans when they employed transparent glass in window covering [24]. This architectural material, however, was available only to the wealthy individuals during that time. It was only in the 19th century that less expensive processes of glassmaking were invented to pave the way for glass to be one of the most remarkable materials in architecture.

One of the most important features of glass is its ability to admit natural light into spaces, which, in addition to contributing to a healthy wellbeing by evoking positive emotions and increasing productivity [25], can lead to significant energy savings during buildings' operation [26]. Due to the increasing demand for reducing energy use in the built environment, which heavily contributes to the world's carbon emissions, several types of energy-efficient

glass, such as low-emissivity (low-e) glass, have emerged to produce windows with improved insulating properties and better energy-loss control [27].

Glass panes used in building façades and windows are usually laminated, meaning they are formed by bonding two separate sheets using a polymer interlayer, such as polyvinyl butyral (PVB) resin [15], which allows for the glass pieces to remain in place when it is broken. Windows can also be constructed using insulating glass units (IGU), which are made up of at least two glass panes separated by an inert gas. This improves the insulating properties of the windows, creating a more energy-efficient envelope.

A glass façade is not considered a part of the building's structural framework; that is, it is not a load-bearing element in the building design [28]. The structural design of glass façades is generally driven by wind load and its own weight. In most cases, the imposed load on the glass is transferred to the building's structural system through a system of aluminium curtain wall, which is a frame consisting of vertical and horizontal components called transoms and mullions, respectively. The frame is connected to the building's structural system through anchors. Figure 2.8 shows an example of a building façade made of glass.



Figure 2.8 Building glass façade in Espoo, Finland.

The use of glass in passenger ships has seen a rapid increase in recent years. Most modern cruise ships have windows that allow the passengers to enjoy a pleasant view as well as provide insulation for the interior to maintain a comfortable temperature. Figure 2.9 [29] shows an example of a modern cruise ship with a large glass dome, which reflects the growing trend in creating large glass façades in ships. Most of the glass used in ship windows is fully tempered, and the windows are made of IGUs for improved insulation properties. The IGUs are either made of a combination of laminated glass and a



Figure 2.9 Cruise ship with a big glass dome [29].

monolithic glass pane, or two laminated glass units [5]. The driving loads for the structural design of ship windows are wind loads for windows in the upper decks and water pressure for those in the lower decks [5]. The primary design value is the flexural strength of glass, which is used to determine the thickness to ensure structural safety. The design of ship glass windows can be carried out following different classifications, such as Bureau Veritas [30] and Lloyd's Register [31].

Recently, glass applications have expanded to include structural elements. There has been hesitation in using glass as a load-bearing element in buildings due to the public perception that glass is fragile and dangerous. Nevertheless, efforts have been made by innovative designers to push the limits of glass and utilize its remarkable mechanical properties by using it as a load-bearing element in buildings and other structures. Glass can be used in buildings as columns, beams, slabs, staircases, or floors. An example of glass being utilized as a beam element is seen in Eindhoven Central Railway Station in the Netherlands (Figure 2.10 [32]). Laminated glass is often used for structural applications for safety reasons [6]. Glass can be used as a structural element either on its own or in combination with other materials such as steel or wood for an improved structural performance. Another innovative application of glass as a load-bearing element can be seen in the Zhangjiajie Bridge in China (Figure 2.11), where the deck of the bridge is made of tempered glass.



Figure 2.10 Glass structural beams in Eindhoven central railway station, The Netherlands [32].



Figure 2.11 Pedestrian bridge with glass deck in Zhangjiajie, China [33].

3 Strength of glass

When glass fails under stress, it fails in a brittle, sudden manner. The European standard EN 5271-1 [34] tabulates the numerical values of all the relevant mechanical properties of glass except its strength, which indicates that glass strength is not as straightforward. Glass's mechanical properties, such as elastic modulus and hardness, are inherent to the material. Glass strength, on the other hand, is dictated by environmental factors rather than intrinsic bond strength between atoms. Glass can withstand much higher compression stresses than tensile stresses. In turn, tensile strength, particularly flexural tensile strength, is of utmost importance for structural applications.

3.1 Theoretical versus practical strength

The minimum stress required to break the atomic bond of a material such that two new surfaces are created is called the theoretical strength. If we consider glass as a flawless material, then its strength would be directly related to the energy required to separate two surfaces due to bond breakage. That was first proposed by Orowan [35] by expressing the Orowan stress (σ_m) as:

$$\sigma_m = \sqrt{\frac{E\gamma}{r_o}}, \quad (2.1)$$

where E is Young's modulus, γ is the fracture surface energy, and r_o is the equilibrium distance between atoms to maintain a bond. To an extent, none of these terms is dependent on the glass composition; thus, the strength obtained through this formula should be somewhat valid for all silicate glasses regardless of their composition. Values of 70 GPa, 3.5 J/m², and 0.2 nm are commonly accepted for silicate glasses for E , γ , and r_o , respectively [14]. Substituting these values into Eq. 2.1 yields that glass strength should be as high as 35 GPa.

The strength of glass used in most practical applications is substantially lower than that calculated from Eq. 2.1. The European standard EN 572-1 [34] quotes the strength of annealed soda-lime-silicate glass as 45 MPa, which is almost eight hundred times lower than the theoretical strength. This immense discrepancy is due to microscopic flaws in the glass surface, which act as stress concentrators and cause the local stress to exceed the theoretical strength [1].

The existence of flaws in glass is inevitable, and their distribution is random. Hence, the strength of glass is statistical. Flaws are generally either in the glass bulk, such as air bubbles that were left unremoved in the fining phase, or surface flaws (i.e., microcracks) that are a result of normal handling of glass. The type, distribution, and size of flaws are dictated by the treatment and manufacturing methods used to produce it. Any contact with a material that has a higher hardness than glass can cause flaws. Chemical attacks and thermal shocks can also generate flaws in glass. This explains the difference in strength usually recorded between the tin side and the air side surfaces of glass through the float process [7,36]. As the two sides undergo different contact scenarios, the distribution and size of flaws vary from each side, which reflects on the fracture strength. Since the surface of freshly produced glass has a particularly large coefficient of friction, it is very susceptible to flaw formation through any contact, which makes the prevention of flaws virtually impossible [1]. Contact-induced flaws, however, can be reduced by applying a lubricant to the surface of freshly produced glass.

Glass strength is not constant as it ages. That is, during the service life of a glass pane, different defectiveness scenarios take place, which cause its strength to deteriorate. The continuous exposure of glass to the atmosphere, as well as the continuous contact with other materials, can cause corrosion and abrasion, which, in turn, leads to a significant strength loss over time [7,14,15].

3.2 Fracture mechanics

The stresses in plates containing cracks were studied by Inglis back in 1913 [37]. He formulated an expression for determining the maximum stress (σ') at the tip of an elliptical hole or flaw within a plate subjected to a uniform tensile stress (σ_a), having a minor dimension $2b$ and a major dimension $2c$, as:

$$\sigma' = \sigma_a \left[1 + \left(\frac{2c}{b} \right) \right]. \quad (3.1)$$

This expression indicates that when σ_{yy} reaches the theoretical strength σ_m , failure will occur. Griffith [38] built on the work of Inglis and, by utilizing the principle of minimum potential energy, developed the foundational fracture energy balance theory. According to the theory, there is a reduction in

potential energy due to crack formation; this reduction is matched by an equivalent increase in strain energy. Griffith energy balance theory is formulated as:

$$\sigma_f = \sqrt{\frac{2E\gamma}{\pi c^*}}, \quad (3.2)$$

where σ_f is the failure stress and c^* is the critical crack length beyond which it will propagate into fracture. This expression hints that fracture is largely driven by the existence of flaws rather than inherent material properties like E and γ . Griffith argues that the fracture will happen due to the most dominant flaw present, analogous to the weakest link in a chain. These flaws are known as Griffith flaws or critical flaws.

Later, the work of Griffith was modified by Irwin [39], who proposed that there are three distinguished displacement modes for crack surfaces relative to each other (Figure 3.1). Mode I (opening mode) involves crack propagation

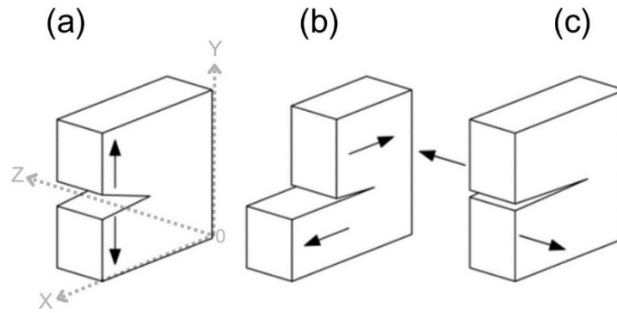


Figure 3.1 The three modes of crack propagation: (a) Mode I: opening; (b) Mode II: sliding; (c) Mode III: tearing [7].

through tensile stresses perpendicular to the crack plane, pulling the crack faces apart. Mode II (sliding mode) involves a shearing action where the applied stress is parallel to the crack plane and thus producing a sliding movement. Mode III (tearing mode) is an out-of-plane shearing mode, where the applied stress is acting parallel to the crack front causing the crack faces to slide over each other in opposite directions.

Irwin associated each crack extension mode with a quantity called stress intensity factor (SIF), which relates to the stress intensity near the tip of a crack. The stress intensity factors for mode I, mode II, and mode III are denoted as K_I , K_{II} , and K_{III} , respectively, and are defined as:

$$K_I = Y\sigma_{yy}\sqrt{\pi c}, \quad (3.3a)$$

$$K_{II} = Y\sigma_{xy}\sqrt{\pi c}, \quad (3.3b)$$

$$K_{III} = Y\sigma_{zy}\sqrt{\pi c}, \quad (3.3c)$$

where Y is a shape factor depending on the shape of the crack (see Table 3.1) and c is the crack depth. Cracks in glass are mostly semi-circular in shape [40], and therefore the value of the shape factor (Y) is usually taken as 0.71 [17]. Failure occurs whenever one of the SIFs reaches a critical value K_{Ic} , K_{IIc} , or K_{IIIc} . Since crack propagation in glass happens primarily through mode I, with the effects of mode II and mode III being negligible [15], K_{Ic} is considered the governing criterion and is known as the fracture toughness; accordingly, here and in what follows, the quantities K_I , K_{Ic} , and σ_{yy} will be referred to as K , K_c , and σ , respectively. Fracture toughness is a material property representing the material's ability to resist crack propagation. The fracture toughness of soda-lime-silicate glass ranges between $0.72 \text{ MPa}\sqrt{m}$ to $0.82 \text{ MPa}\sqrt{m}$ [17,41]. According to Eq. 3.3a, the critical crack depth c_{cr} and the critical stress σ_{cr} can be expressed explicitly as:

$$c_{cr} = \left(\frac{K_c}{\sigma Y \sqrt{\pi}} \right)^2, \quad (3.4a)$$

$$\sigma_{cr} = \frac{K_c}{Y \sqrt{\pi c}}. \quad (3.4b)$$

Table 3.1 Shape factor- Y for commonly occurring cracks in glass [17].

Crack description	Shape factor (Y)
Elliptical crack	0.637
Vickers indentation	0.666
Glass-on-glass scratching	0.564
Semi-circular	0.713
Surface crack on a semi-infinite specimen	1.120
Quarter-circle crack on the glass edge	0.722
Sandpaper scratching	0.999

Nonetheless, cracks in glass can propagate under an applied stress that is much smaller than the critical limit predicted by Eq. 3.4b. This can be traced to a phenomenon known as static fatigue or subcritical crack growth. This phenomenon is time-dependent, and it occurs due to a chemical reaction between glass and the water in the surrounding environment. The effect of this phenomenon reaches its maximum extent in environments where glass is surrounded by water [9], and it can therefore be more pronounced in applications such as ship or submarine windows. This chemical reaction aggravates crack growth. The rate and intensity of the reaction increase with stress; thus, the reaction rate is highest near the crack tip, which implies a dependence on the SIF. The relationship between crack growth rate and the SIF is expressed as [42]:

$$\frac{dc}{dt} = v_o \left(\frac{K}{K_c} \right)^n, \quad (3.5)$$

where v_o and n are crack velocity parameters depending on the test conditions, temperature, relative humidity, and type of glass; the values of these parameters are discussed in detail by Haldimann [17]. To take time

dependency into account in Eq. 3.4a and Eq. 3.4b, the differential equation 3.5 is solved (the derivation is available in [17]), obtaining the crack depth $c(t)$ and the stress $\sigma(t)$ as:

$$c(t) = \left(c_i^{\frac{2-n}{2}} + \frac{2-n}{2} v_o k_c^{-n} (Y\sqrt{\pi})^n \int_0^t \sigma(\tau) d\tau \right)^{\frac{2}{2-n}}, \quad (3.6a)$$

$$\sigma(t) = \left(\frac{2}{t^{(n-2)v_o k_c^{-n} (Y\sqrt{\pi})^n c_i^{\frac{n-2}{2}}} \right)^{\frac{1}{n}}, \quad (3.6b)$$

where c_i is the initial crack depth, t is a specific point in time, and τ is the time variable. Failure occurs when the stress $\sigma(t)$ at the crack location reaches a critical value σ_{cr} as the crack depth $c(t)$ reaches $c_{cr}(t)$ at failure time t_f .

3.3 Statistical interpretations of glass strength

As a result of being driven by random variables, i.e., distribution, severity, and orientation of flaws present on its surface, the strength values of seemingly identical glass panes are highly scattered, which entails a statistical analysis. Like any other continuous random variable, glass strength needs to be described using a probability density function (PDF) for estimating the probability of failure under a specific stress. Common probability distributions used to describe glass strength are Weibull, normal, and log-normal distributions. Traditionally, the two-parameter Weibull distribution, described in the European standard EN 12603 [43], is most commonly used to model glass strength; however, the goodness-of-fit of the model to the strength data is not always satisfactory. In such cases, another distribution should then be considered for modelling the strength data.

Since its introduction in 1939 [44], the Weibull statistical model has been used extensively to characterize the strength of brittle materials. The appeal of the model stems from its high flexibility that allows it to take different forms and shapes, its simple mathematical formula, and having a closed form cumulative distribution function (CDF). The model holds that the material will fail due to the most critical flaw present (weakest link concept). The use of the Weibull model for analysing material strength requires the flaws being randomly distributed without having a preferential orientation or location, with individual flaws not affecting one another; these conditions can reasonably be assumed to be met in the case of glass [17].

The surface flaw distribution on a glass sheet of an area A can be statistically described by a function $f(c)$. For any infinitesimally small area dA , the probability of having a flaw of depth c or larger is $f(c) \cdot dA$. If the area A is divided into a number (n) of small areas A/n , it follows that there will be no flaws of depth c or larger in area A in case none of the small areas A/n has any. Since

the probability of a small area A/n having a flaw of depth c or larger is given by $f(c) \cdot A/n$, the probability of it not having that kind of flaw is, in turn, $1 - f(c) \cdot A/n$. For the entire area A with a large number of small areas, the probability of not having a flaw of depth c or larger is given as:

$$\lim_{n \rightarrow \infty} \left(1 - f(c) \frac{A}{n}\right)^n = e^{-Af(c)}. \quad (3.7)$$

Accordingly, the probability of the area A having a flaw of depth c or larger is the complementary of Eq. 3.7. The distribution function $f(c)$ has to be a positive, nondecreasing function, vanishing at a specific value x_0 ; the simplest function to satisfy these conditions is of the form $\frac{(c - x_0)^\beta}{\theta}$, where β , θ , and x_0 are constants while c relates to the stress intensity factor K as described previously in Eq. 3.3a. Failure occurs when K reaches the fracture toughness K_c as the critical flaw depth c_{cr} is reached. The relationship between the critical crack depth and the critical stress σ_{cr} was described in Eq. 3.4a and Eq. 3.4b. Following that, it can be said that the probability of failure (P_f) of a glass sheet of area A under a stress σ_{cr} (i.e., area A having a critical flaw) is expressed as:

$$P_f = 1 - \exp \left[- \left(\frac{\sigma_{cr} - x_0}{\theta} \right)^\beta \right]. \quad (3.8)$$

This function is the general CDF of the Weibull distribution; it is known as the three-parameter Weibull function. The constants β , θ , and x_0 are referred to as the Weibull parameters: β is the shape parameter, θ is the scale parameter, and x_0 is the location parameter of the distribution. It should be noted that the area term A in Eq. 3.7 is implicitly accounted for as a part of the parameter θ . The location parameter x_0 represents a specific stress threshold below which the material cannot fail. If there is no clear lower bound for the strength of brittle materials, the location parameter is conventionally assumed to be zero for safety concerns, according to Trustrum and Jayatilaka [45]. That being the case, the expression in Eq. 3.8 is reduced to represent the two-parameter Weibull function:

$$P_f = 1 - \exp \left[- \left(\frac{\sigma_{cr}}{\theta} \right)^\beta \right]. \quad (3.9)$$

The goodness-of-fit of the model to the strength data is assessed by plotting a linearized form of Eq. 3.9 against the glass strength data. The linearized form is achieved by taking the natural logarithm twice on each side, yielding:

$$\ln \left(\ln \left(\frac{1}{1 - P_f} \right) \right) = \beta \ln \sigma_{cr} - \beta \ln \theta. \quad (3.10)$$

An example of a linear plot of the two-parameter Weibull distribution of glass strength samples is shown in Figure 3.2, where $\ln \left(\ln \left(\frac{1}{1 - P_f} \right) \right)$ is on the y-axis and $\ln \sigma_{cr}$ is on the x-axis.

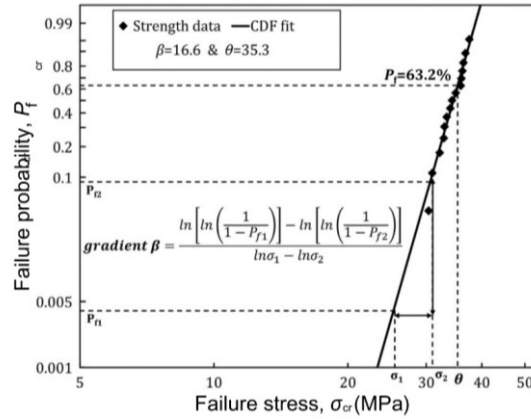


Figure 3.2 Linearized two-parameter Weibull distribution of glass strength [46].

The Weibull parameters, β and θ , can be determined graphically from the linear plot: The shape parameter beta represents the slope of the line, and the intercept is $-\beta \cdot \ln \theta$. The shape parameter β is a measure of the scatter of the data around the line. The higher the value of this parameter, the less scattered the data are. Values of β for soda-line-silicate glass typically range from 5 to 15 [46]; a too small value of β could imply that the distribution is not a good descriptor of the data, and another distribution should be considered. The scale parameter, θ , represents the stress level that would cause 63.2% of the specimens to fail. That is, when the stress σ_{cr} becomes equal to θ , the failure probability reads $P_f = 1 - e^{-1} = 0.632$.

While graphical estimation of the Weibull parameters can be simple and convenient, this method, however, does not provide the most accurate results. Therefore, there exist in the literature various methods for estimating the Weibull parameters. They can be categorized as either manual methods or nonlinear computational methods. The most common manual methods are the methods of least squares and weighted least squares regression, while the most common computational methods are the method of moments and the method of maximum likelihood estimation. Datsiou and Overend [46] made a study comparing the efficacy of these methods for analysing glass strength data. They concluded that the weighted least squares method provides the best goodness-of-fit to the Weibull distribution, as well as being simpler to implement compared to the nonlinear computational methods.

The described Weibull model assumes that there is only one population of flaws that drives the glass failure. Nevertheless, if there are two distinct flaw populations present that drive two independent failure mechanisms, then a bimodal Weibull model, where the plot has two straight lines instead of one, is used to analyse glass strength.

Pisano [7] mentions that glass, in fact, cannot fail under a certain stress limit. This is a result of quality control measures done by glass manufacturers during the float process that involve discarding any glass sheet that has a flaw

exceeding certain dimensions. And since the strength is almost exclusively controlled by flaw size, ensuring it has a maximum limit essentially sets a lower bound for the strength. Hence, the three-parameter Weibull or the left-truncated Weibull distributions represent more appropriate models to study glass strength. The two models are similar to each other, with the most notable difference being the physical meaning behind the location parameter x_0 . In the three-parameter Weibull model, x_0 is an intrinsic property of the material; on the other hand, in the left-truncated Weibull model, x_0 comes from a selection process that rejects any specimen with a strength lower than that specific limit. These bounded models work best for glass tested on its airside. For tin side strength, Pisano suggests using a bimodal left-truncated Weibull distribution.

Although many experiments available in the literature suggest that glass strength data will likely fit into the Weibull distribution [3,10,47], Haldimann [17] argues that the two-parameter Weibull distribution fits poorly to strength data of as-received glass specimens obtained from tests conducted under normal temperature, humidity, and atmospheric pressure (i.e., ambient conditions). The distribution, however, will perfectly describe strength data obtained under inert conditions (i.e., in vacuum). He attributes that behaviour to the phenomenon of static fatigue, where he concludes that the goodness-of-fit of the Weibull model deteriorates as the effect of the static fatigue becomes more pronounced. Haldimann developed a lifetime prediction model, based on fracture mechanics and the theory of probability, as an alternative to the commonly used Weibull model. He suggests that this model is more appropriate for describing the ambient strength of glass, as well as for the cases with complex stress fields (e.g., tests performed on specimens with large surface area, which involve nonlinear behaviour). The model can be used to predict the time-dependent failure probability of glass elements subjected to a given stress, or the maximum stress the glass can withstand for a specific failure probability. Unlike the other available models used for glass strength prediction, the lifetime prediction model considers all the factors that influence glass strength over its lifetime, including time-dependent loading, static fatigue, non-uniform stress fields, and arbitrary geometries. The generalized form of the model is formulated as:

$$P_f(t) = 1 - \exp \left[- \frac{1}{A_o} \int_A \frac{2}{\pi} \int_{\varphi=0}^{\frac{\pi}{2}} \left(\max \left\{ \left(\frac{\sigma_n(\tau, \vec{r}, \varphi)}{\theta_o} \right)^{n-2} + \left(\frac{1}{U \cdot \theta_o^{n-2}} \int_0^\tau \sigma_n^n(\tilde{\tau}, \vec{r}, \varphi) d\tilde{\tau} \right) \right\} \right)^{\frac{1}{n-2}} \right]^{m_o} dA d\varphi, \quad (4.11a)$$

$$\text{where} \quad U = \frac{2k_c^2}{(n-2)v_o Y^2 \pi}, \quad (4.11b)$$

where A_o is a unit surface area, t is a point in time, $\sigma_n(\tau, \vec{r}, \varphi)$ is the stress component perpendicular to the crack orientation φ at point \vec{r} (x, y) at time

τ , θ_0 and m_0 are the Weibull parameters representing the surface conditions, U is a coefficient accounting for static fatigue, n and v_0 are the crack velocity parameters, and Y is the geometry factor. This model combines all the parameters previously featured in separate equations from different contexts (i.e., Eq. 3.4: fracture mechanics, Eq. 3.5: static fatigue & Eq. 3.8: Weibull distribution). A detailed approach for the determination of the model parameters is available in [17]. The model can be further simplified for cases where a uniform stress field can be assumed and for cases with constant loading.

3.4 Testing methods of glass strength

Flexural tensile strength is the main subject of interest in the context of glass structural performance. Testing methods used to evaluate glass strength can either produce a uniaxial stress or a biaxial stress on the glass tensile surface. There are several testing methods used for determining glass strength, the most common of which are the four-point bending test and the coaxial double ring test. Tests can be conducted under ambient conditions (i.e., normal temperature, humidity, and atmospheric pressure) or inert conditions (i.e., vacuum or a completely dry medium). Testing under inert conditions rules out the effect of static fatigue, and the strength obtained from these tests is called the inert strength. The effect of static fatigue can also be significantly reduced under ambient conditions for dried specimens tested at a very rapid loading rate (20 MPa/s) [17]. The bulk of glass tests, however, have been conducted under ambient conditions. This is because achieving inert or near-inert conditions can be difficult or expensive. Additionally, testing under ambient conditions is more reflective of service conditions of glass, and the results are therefore more representative of the material's real structural performance in practical applications.

Four-point bending test:

The four-point bending test (4PB) is a standardized test for testing glass strength by the European standard EN 1288-3 [48]. A schematic representation of the test is illustrated in Figure 3.3. The test involves a uniaxial bending of a simply supported rectangular glass specimen using two rollers pushed down simultaneously by a controlled force. The standard dimensions of the specimens are $1100 \pm 5 \text{ mm} \times 360 \pm 5 \text{ mm}$. There are four points of contact in the test: two between the specimen and the load rollers and two between the specimen and the supports. Rubber is placed at these points to minimize stress concentration. The test is conducted under ambient conditions with a temperature of $23 \pm 5 \text{ }^\circ\text{C}$ and a relative humidity between 40% and 70%. The specimen is monotonically loaded with a constant bending stress rate of $2 \pm 0.4 \text{ MPa/s}$ until failure.

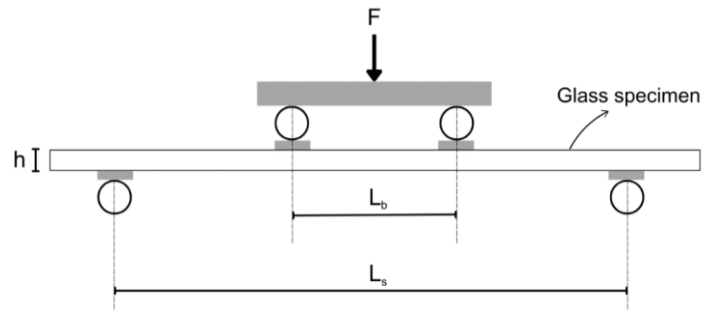


Figure 3.3 Four-point bending test; $L_b = 200 \pm 1$ mm and $L_s = 1000 \pm 1$ mm, as per the European standard EN 1288-3.

This test is preferred to the three-point bending test, which only involves one load bearing at the center, because it creates a uniform maximum tensile stress on the bottom surface of the specimen between the two load rollers, which increases the surface area subjected to maximum stress, increasing the probability of realizing a critical flaw. The 4PB test has been widely used by researchers to evaluate glass strength [3,4]. However, it has the drawback of including edge effects, which could significantly influence the glass failure strength. That is, the configuration of the test warrants that both the edges and the surface are subjected to maximum stress along the central span. The edges are problematic because they are susceptible to additional flaws during the cutting process. Hence, this test is only favoured when determining the strength of glass in applications where the edge effects are important.

Coaxial double ring test:

The coaxial double ring (CDR) test, also known as the ring-on-ring test, is a testing method with a rotationally symmetric setup that involves two concentric rings acting as a supporting ring and a loading ring. Unlike the 4PB test, the CDR test aims to produce an equibiaxial stress field inside the circular area confined by the loading ring that is sufficiently far from the edges of the specimen, thus ruling out the edge effects. In addition, the directionally independent stress state produced by this test ensures that all the flaws are subjected to a maximum stress that is normal to the direction of the flaw plane, which, in turn, increases the probability of catching the most critical flaw present.

The test is standardized by the European standards EN 1288-2 [49] and EN 1288-4 [50] for glass elements with large test area and small test area, respectively. For glass specimens with small test area, the test setup proposed by EN 1288-4 involves placing a square or circular glass specimen on a supporting ring of radius r_1 while applying a downward load F through a concentric loading ring of radius r_2 (where $r_2 < r_1$). Figure 3.4a shows a schematic representation of the test configuration. The test is conducted under the same ambient conditions specified for the 4pb test with the same bending stress rate [50]. Since the stress should be maximum within the area delimited by

the loading ring and subside moving towards the edges, failure should occur within this area. That is, any failure happening at the periphery or outside of the loading ring is either due to undesired stress concentration or an incorrect test setup. This test configuration has been used numerously to determine glass strength [10,51] as a result of being relatively easy and inexpensive to perform. Nonetheless, the size of the test area specified for this test configuration is rather too small to accurately represent the actual strength of glass. Hence, this test often overestimates the strength of glass, as the probability of realizing critical flaws increases as the test area increases. On that account, the standard EN 1288-2 proposes a test setup for testing specimens with large test areas. The test setup is similar to that proposed in EN 1288-4, except for an additional overpressure P that is applied in the same direction as the loading (Figure 3.4b). This overpressure is supposed to be adjusted with respect to the force F to compensate for the geometric nonlinear effects that occur as plates undergo large deformations [7, 51]. That is, as the effects of geometric nonlinearities become more significant, the equibiaxial stress state is disturbed, and an undesired localized stress starts to develop along the contact circle of the loading ring [8]. In this case, the stress calculation using the simple bending theory is no longer accurate. Many researchers, however, mentioned that this test setup is overly sophisticated and difficult to perform [7,10,51], as well as not being able to fully compensate for the geometric nonlinear effects and maintain an equibiaxial stress state [11,12].

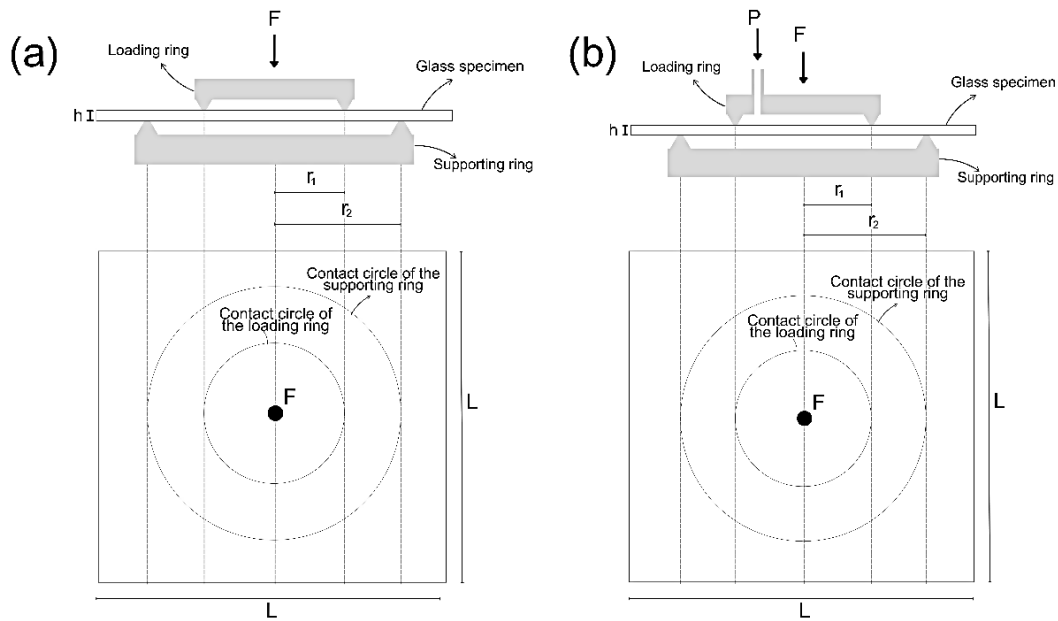


Figure 3.4 Coaxial double ring test: (a) test setup for specimens with a small test area; (b) test setup for specimens with a large test area.

Effects of geometric nonlinearity:

Since the thickness of glass panes is small compared to the other dimensions, they can be described by thin plate models. Whenever thin plates undergo deflections (w) close to their thickness (h), a stretching action of the middle surface, known as the membrane effect, starts to accompany the bending stresses. As the deflection increases to exceed the plate thickness ($w > h$), the membrane emerges as the predominant load-carrying mechanism of the plate [13]; these plates are known as flexible plates. The relationship between the strain and deflection then takes a nonlinear form, which is referred to as geometric nonlinearity. Linear plate theories (e.g., Kirchhoff-Love plate theory, Mindlin-Reissner plate theory, etc.) do not account for the membrane action, assuming that the middle surface remains unstrained after bending, and only consider the bending stresses [13]; therefore, they tend to overstate the flexural stress in cases where plates are undergoing large deflections. Geometric nonlinearity is a favourable behaviour as it offers an additional resistance to lateral loads; however, nonlinear analysis of plates tends to be more complex. For plates undergoing small strains and moderate rotations of the normal to the mid-surface (10° to 15°), the nonlinear relationship between strains (ϵ) and displacements can be described by including the Von Karman strains (the nonlinear terms) into the classical Kirchhoff-Love equations. In Cartesian coordinates (where x and y are the in-plane directions and z is the transverse direction), the strain-displacement relationship is expressed as [13]:

$$\epsilon_{xx} = \frac{\partial u_0}{\partial x} + \frac{1}{2} \left(\frac{\partial \omega_0}{\partial x} \right)^2 - z \frac{\partial^2 \omega_0}{\partial x^2}, \quad (4.1a)$$

$$\epsilon_{yy} = \frac{\partial v_0}{\partial y} + \frac{1}{2} \left(\frac{\partial \omega_0}{\partial y} \right)^2 - z \frac{\partial^2 \omega_0}{\partial y^2}, \quad (4.1b)$$

$$\epsilon_{xy} = \frac{1}{2} \left(\frac{\partial u_0}{\partial y} + \frac{\partial v_0}{\partial x} \right) + \frac{1}{2} \left(\frac{\partial \omega_0}{\partial x} \frac{\partial \omega_0}{\partial y} \right) - z \frac{\partial^2 \omega_0}{\partial x \partial y}, \quad (4.1c)$$

where u_0 , v_0 , and ω_0 are the mid-surface displacement components in x -, y -, and z -directions, respectively. The first two terms in the equations relate to the membrane strains, while the last term (involving second derivatives) relates to the bending strains. In the above equations, the in-plane strains are coupled with the transverse displacement through the nonlinear terms, meaning that the stretching (membrane) and bending problems cannot be solved separately.

Since the CDR test configuration involves an axisymmetric circular loading, and sometimes circular glass specimens, polar coordinates are used for modelling such plates. Considering radial coordinates, the in-plane strain components in the radial and tangential directions (ϵ_r and ϵ_t respectively) as well as the mid-surface curvature in the radial and tangential directions (χ_r and χ_t

respectively) for axisymmetric bending of a circular plate of radius r are expressed as [13]:

$$\epsilon_r = \frac{du}{dr} + \frac{1}{2} \left(\frac{d\omega}{dr} \right)^2, \quad (4.2a)$$

$$\epsilon_t = \frac{u}{r}, \quad (4.2b)$$

$$\chi_r = -\frac{d^2\omega}{dr^2}, \quad (4.2c)$$

$$\chi_t = -\frac{1}{r} \frac{d\omega}{dr}, \quad (4.2d)$$

where u and ω are the radial and normal displacements of the mid-surface. The analytical solution for plates undergoing large deflections tends to be very complex, and therefore numerical methods, such as the finite element method, are often utilized to analyse such plates.

4 Experimental program

A set of laboratory tests is conducted on glass specimens using a novel setup for the CDR test. The proposed setup is intended to be a simpler alternative to that specified in EN 1288-2, where only a uniform water pressure is applied instead of a combination of water pressure and ring-loading. The testing method aims to promote the development of geometric nonlinearity by subjecting a large area to biaxial stress. The tests are conducted under ambient conditions to be more reflective of the glass's structural performance under use conditions. 21 fully tempered glass specimens with identical nominal dimensions are tested, and the results are recorded with the aim of developing the optimal test setup that is able to consistently produce valid tests for the majority of trials. There are three main criteria for a test to be considered valid:

- The location of the failure origin should be within the loaded area.
- Minimal to no water leakage should take place in the system.
- The load-displacement relationship is consistent with the general pattern exhibited by the majority of the specimens.

4.1 Test setup

The main components of the test apparatus are two concentric steel rings of equal diameter, between which the specimen is placed, and a water pressure control system. The rings are 800 mm in diameter. Figure 4.1 shows a schematic representation of the test.

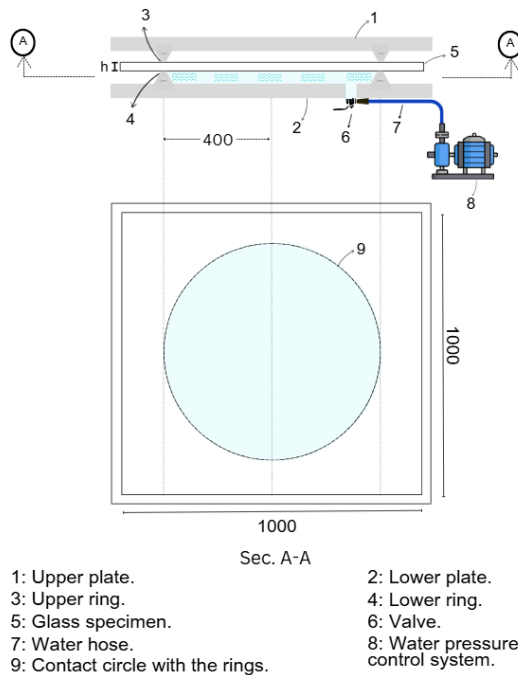


Figure 4.1 Schematic of the test setup (dimensions in mm).

The glass specimen is placed so that it is concentric with the two rings. The concentricity of the rings is achieved through steel angles. This method ensures that the eccentricity stays within 2 mm, which was proven acceptable through iterations. In addition, geometry scans of the test setup were performed for multiple tests to verify that the eccentricity is within an acceptable range.

The stress is induced into the specimen only through a uniform water pressure applied upwards on the bottom surface. The water pressure increases linearly until the glass fails. An adhesive safety film is placed on the compression (lower) surface of the specimen to keep the glass in place after failure. Two rubber rings with varying stiffnesses are placed between the glass and the steel rings. This configuration is chosen based on several trials and errors. More information about the specifications of the rubbers is provided in Section 4.7. The lower rubbers are secured in place by being screwed to the bottom steel plate. A lubricant (petroleum jelly) is applied between the rubber and the glass to reduce friction; these measures are meant to minimize localized contact stresses. The lower cavity, delimited by the glass specimen and the lower ring, is filled with water. The water pressure is managed through a proportional-integral-derivative (PID) controller. A tank placed next to the test setup serves as the water source. The tank is connected to a valve fitted to an opening in the lower ring, as shown in Figure 4.1. The PID system is tuned so that the pressure increases linearly until it reaches a target point below which the failure is expected to occur. A picture of the test setup is shown in Figure 4.2.

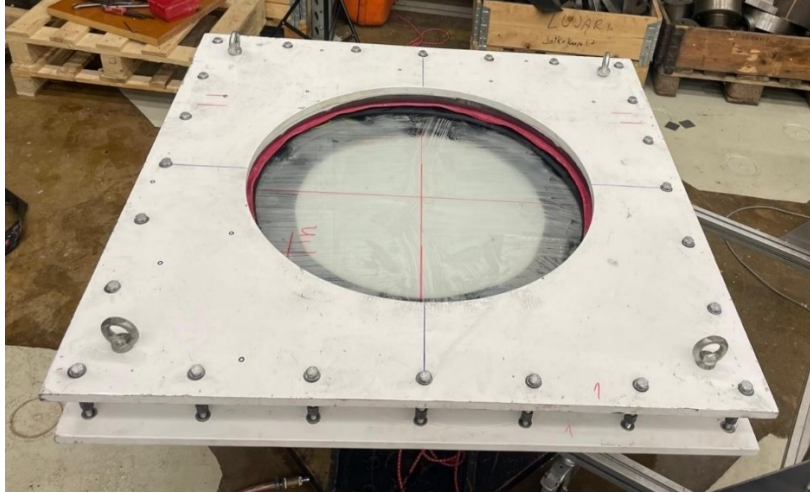


Figure 4.2 Test setup.

4.2 Test specimens and preparations

A total of 21 specimens with nominal dimensions $1000 \times 1000 \times 6$ mm are tested. The specimens are made of soda-lime-silicate glass and are fully tempered. The size of the specimens is large enough so that the effect of geometric nonlinearity is significant when undergoing biaxial bending. The specimens were produced by the Finnish supplier Jaakko-Tuote Oy. All specimens were subjected to the same manufacturing processes, treatment, and storage conditions. Figure 4.3 shows the test specimens stored at ambient conditions (relative humidity between 25% and 50% and temperature around 20 °C) in the laboratory where the testing is taking place. The specimens are stored vertically with cork separators in between them to minimize scratching and avoid introducing additional surface flaws. Specimen preparations include assigning a specimen identifier, measuring the thickness using a digital glass thickness meter device, drawing center lines to serve as X- and Y-local axes for reference, and installing a membrane film on the specimens' compression side.



Figure 4.3 Test specimens

Since, as discussed in Section 3.1, glass tends to show different strengths depending on which side it is being tested, all the 21 specimens are tested on their tin side for consistency. A tin-side detection device (Aoptek model TS580) is used to identify the tin side of each glass pane by exposing it to a short-wave UV light. When the device is facing the tin side, a white, milky background is visible in the device screen; this white background is absent when the device is in contact with the air side. Figure 4.4 shows the device in operation. The tin side detection test is done before each specimen is tested.

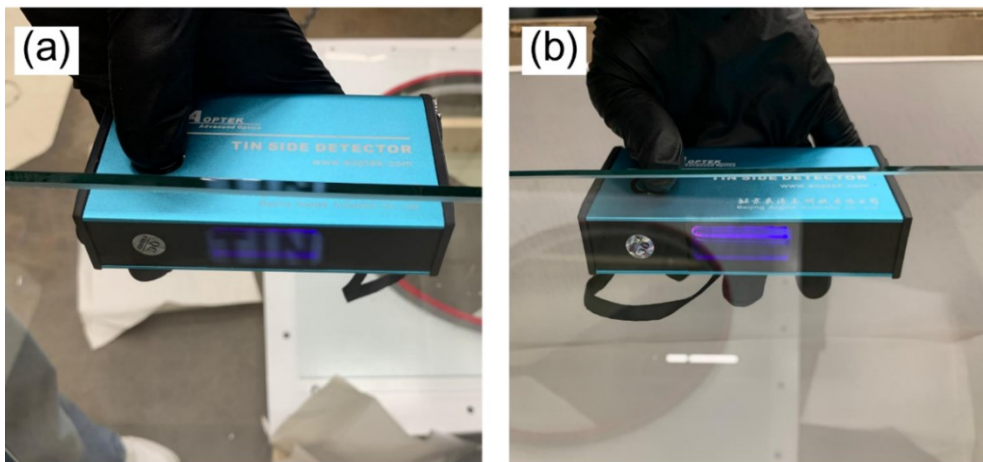


Figure 4.4 Tin side detection test: (a) tin side of the glass with a white background; (b) air side of the glass with no white background.

4.3 Pressure control system

The water pressure is managed through a PID controller. The goal is to increase the pressure linearly until it reaches a specified target pressure. Based on multiple tests and refinements, a target pressure of 2.4 bar was found to be suitable, as nearly all the specimens failed below this limit.

Controlling the system involves three different software: Arduino IDE for developing and compiling the PID control code, QTSerialMonitor for controlling the PID coefficients, specifying the pressure target point, and monitoring the real-time pressure response, and finally, Catman Data Acquisition software is used for recording and saving the data. The source code implemented in Arduino IDE is available in Appendix B.

The PID parameters are tuned to achieve a smooth, linear transition in water pressure from 0 to 2.4 bar. Three coefficients in the PID algorithm can be adjusted with respect to each other to achieve the best response for a specific system. The three coefficients are the proportional (k_p), Integral (k_i), and derivative (k_d). k_p and k_i are the only relevant coefficients for tuning this experiment, and therefore k_d will be kept at 0. Different combinations for k_p and k_i were evaluated for a ramping time of 200 seconds. With trial and error, it became evident that the combination $k_p=1400$ and $k_i=800$ provided the most

stable response with the least fluctuations. However, to avoid having a steep jump in pressure at the initial part of the response, the response is divided into two phases. The first phase is meant to stabilize the system, where a relatively low target pressure of 0.1 bar is specified. After the water pressure reaches the contrived target point and becomes stable, the actual desired target pressure of 2.4 bar is specified. This strategy ensures a smoother and more stable response throughout the loading period.

4.4 Data acquisition

The main variables of interest in this experiment are the water pressure, time to failure, central displacement, and in-plane strains. For the majority of the tests, only the central displacement and the water pressure are recorded. In a subset of tests, however, strain gauges (SG) and Digital image correlation (DIC) are utilized. WIKA pressure sensor of model A-10 is used to monitor the water pressure. The sensor measures pressure from 0 bar up to 2.5 bar with an error range between 0.1% and 0.2%. HBM inductive displacement sensor model WA/50mm is used to measure the central deflection of the glass specimen. The pressure sensor and the displacement sensor are connected to QuantumX MX410B universal amplifier to ensure a precise real-time data acquisition.

Strain gauges:

In addition to measuring the water pressure and the central displacement, one test features strain gauges, two tests use DIC, and one test combines both. The simultaneous use of the DIC and strain gauges is for the sake of validation and comparison of results. Strain gauges are used in pairs, where they are placed in opposite quadrants at an angle of 45° , at 23 cm radial distance (see Figure 4.5). Ideally, the location of a strain gauge should be as close as possible to the failure origin. Accordingly, based on tracking failure origin for multiple valid tests, this placement configuration was opted for. The used strain gauges are the so-called 3-grid rosette from HBM, where each strain gauge has three measuring grids: two at a 90° angle that are placed parallel to the X- and Y- axes assigned to the specimen, and one in the middle at 45° . Each grid measures the in-plane strain in its direction. The three strains are designated as ε_a , ε_b , and ε_c . These strains are used to determine the major and minor principal stresses (σ_1 and σ_2 respectively) using the following expressions:

$$\sigma_1 = \frac{E}{1-\nu} \cdot \frac{\varepsilon_a + \varepsilon_c}{2} + \frac{E}{\sqrt{2(1+\nu)}} \cdot \sqrt{(\varepsilon_a - \varepsilon_b)^2 + (\varepsilon_c - \varepsilon_b)^2}, \quad (5.1a)$$

$$\sigma_2 = \frac{E}{1-\nu} \cdot \frac{\varepsilon_a + \varepsilon_c}{2} - \frac{E}{\sqrt{2(1+\nu)}} \cdot \sqrt{(\varepsilon_a - \varepsilon_b)^2 + (\varepsilon_c - \varepsilon_b)^2}, \quad (5.1b)$$

where E is the young's modulus and ν is the Poisson's ratio of glass. σ_1 represents the maximum normal stress within the specimen, where the shear

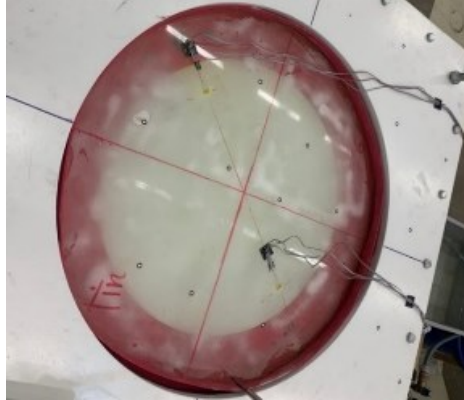


Figure 4.5 Test specimen showing the placement of strain gauges.

stresses vanish. And since the failure is expected to happen when a critical flaw is present in an area where the stress is at its peak, the parameter σ_1 is of utmost importance in this experiment. Since it will be only possible to directly determine the value of σ_1 in tests where strain gauges or DIC were used, its value will be deduced for the rest of the tests, given a similar load-deflection relationship. This is justified by the linear-elastic behavior of glass and the consistency of the boundary and loading conditions.

Digital Image Correlation (DIC):

The DIC system involves two cameras mounted on a tripod, each camera is horizontally rotated 25° inwards. The cameras are of model Basler boA5328-100cm. The cameras were equipped with Schneider-Kreuznach JADE 2.8/16 C lenses. VIC-Snap software by Correlated Solutions is used for the system calibration as well as image acquisition, while VIC-3D software is used for image processing and strain analysis. The DIC calibration is carried out using laser-marked calibration targets. In order to utilize the DIC system, speckle pattern of size 2.54 mm is applied to the specimen surface using ink and a roller. The surface was sprayed with a white scanning spray beforehand to ensure sufficient contrast between the speckle and the surface. This was the case for the first two specimens tested with DIC. For the last specimen, however, fluorescent speckle pattern with speckle size of 1.27 mm was used instead of ink speckle to improve contrast and image resolution. Suitable band-pass filters were used for the cameras to capture only the fluorescent emission and suppress ambient light. The ink speckle pattern was also applied to top surface of the steel frame, so as to allow for inspecting potential rigid body motion that could influence the specimen behavior. Figure 4.6 shows a comparison between the ink and the fluorescent speckle pattern. It can also be seen that two strain gauges were installed for that test. Blue-X-Focus LED light source, mounted in between the two cameras, was used to illuminate the surface of the specimen during testing. For the last test, A white spectrum high-power 500W LED light source was used for obtaining calibration images when the bandpass filters were used for the fluorescent pattern.

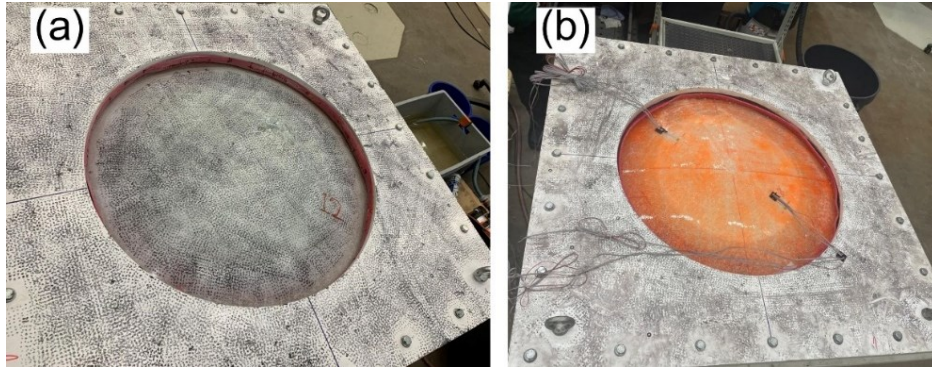


Figure 4.6 Speckle pattern applied on the specimen surface: (a) ink speckle; (b) fluorescent speckle.

4.5 Locating the failure origin

Identifying the location of the failure origin is crucial not only for assessing the validity of the test, but also to track any potential patterns or preferential locations for the failure. Failure must originate from within the loaded area, not along the contact circle, for a test to be considered valid. As discussed in Chapter 3, failure typically happens due to tensile stresses that are concentrated at a critical flaw, which manifests as the failure origin. Upon fracture, tempered glass produces a multitude of small individual pieces due to the internal compressive stresses stored within its surface.

Identifying the origin of failure can sometimes be challenging. If, however, the specimen has remained in place with the majority of the fragments maintained their original position, it can be a fairly simple task with visual inspection. The membrane film adhered to the compression surface of the specimen is critical for that purpose. The failure origin can be identified by observing the fracture pattern. Typically, the fracture pattern involves radial cracks that propagate from the failure origin. Figure 4.7a shows an example fracture pattern where the origin is easily detectable.

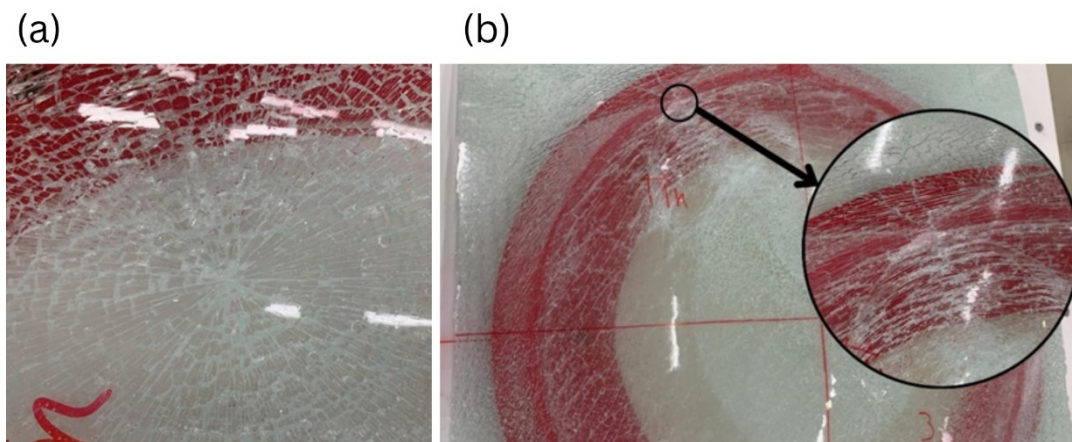


Figure 4.7 Fracture pattern of glass: (a) radial fracture pattern; (b) fracture pattern associated with ring failures.

Nonetheless, the radial failure pattern shown in Figure 4.7a only occurs when the specimen fails from within the loaded area; that is, in essence, when the failure is primarily driven by a somewhat uniformly distributed in-plane stress. In case of contact failure, though, where there is an intense stress concentration along the contact circle, it was observed that the fracture pattern takes a circular form along the fracture surface, forming a shape close to a “stretched x ” around the fracture origin. Figure 4.7b shows the fracture pattern of a specimen that failed along the contact circle. This kind of failure origin is relatively more challenging to locate in the beginning, but it is still a manageable task for an engineer or a material scientist with some amount of experience.

It is not always the case that identifying the location of the failure origin is as straightforward, for example, due to a large part around the origin location being ejected due to the sudden release of stress. Therefore, high-speed photography was utilized to capture the glass failure for the sake of verifying the failure origin location in such cases. As soda-lime-silicate glass can have a terminal velocity reaching 1500 m/s [52], high-speed cameras capable of filming with a frame rate of 20000 frames per second (fps) should be reasonably sufficient to capture where the crack originates and its propagation. For most of the tests, two Mikrotrotron EoSens 2.0CXP2 cameras were used jointly. Triggering of cameras was done with an in-house National Instruments compactRIO based TTL triggering system, operating at 40 MHz clock rate for high precision. Each camera can film with a frame rate of 10000 fps in opposite phase; this results in an effective frame rate of 20000 fps from the two cameras, albeit from slightly different perspectives. The glass was illuminated by three Blue-X focus LED light sources, and later on by a white spectrum high-power 500W LED light source to provide sufficient illumination. Due to power limitations of the blue-x focus in pulsed mode, an exposure time of 17 μ s was used which underexposed the images, while 50 μ s was used with the high-power light source, enabling the use of the sensor’s full dynamic range.

For a few tests, a more sophisticated ultra-high-speed camera (Phantom V2012) was used. The camera was able to record glass failure at a frame rate of 55000 fps, which was more than adequate for capturing crack initiation and propagation. The high-power LED light source was used with the Phantom camera. Figure 4.8 shows the crack propagation captured by the Phantom V2012 camera, where the time difference between individual images b is approximately 18 μ s. The software provided by the manufacturer was used for saving and post-processing the images from the camera.

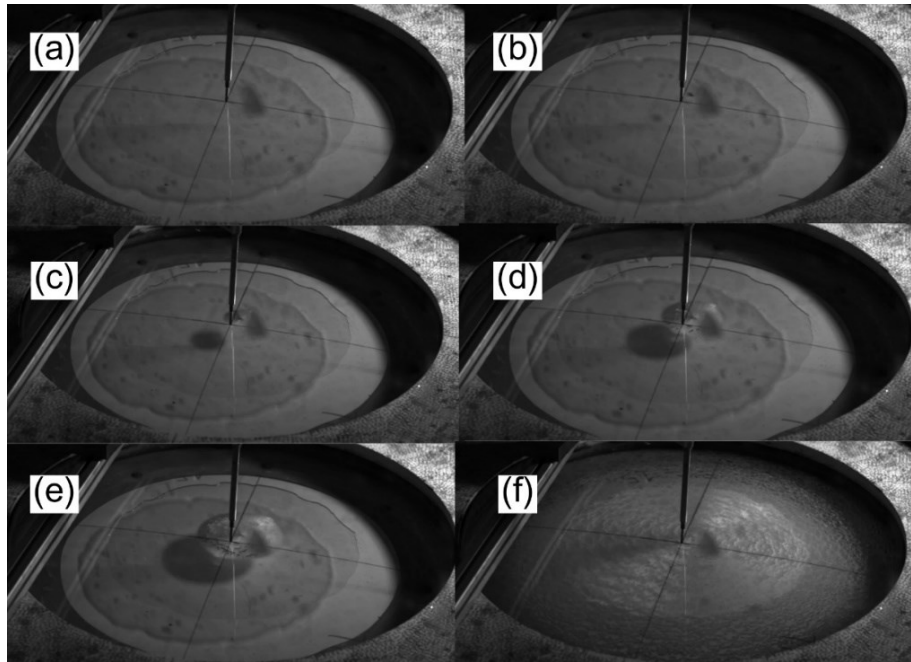


Figure 4.8 Crack propagation captured by the Phantom V2012 camera: (a) specimen before fracture; (b) first frame (crack initiation); (c) second frame of the crack propagation; (d) third frame of crack propagation; (e) fourth frame of crack propagation; (f) specimen in its post-fracture state.

4.6 Error minimization measures

Experimental tests inherently involve some degree of error. The influence of errors that occur systematically can be minimised or somewhat eliminated. It should be noted, however, that deliberate modifications or refinements to the test setup are not considered errors, but rather are part of the test development. Whilst these refinements might have altered the results in some ways, they did not introduce a clear systematic bias. Adding to that, the way in which a specific modification on the test setup affects the glass behaviour might not be completely clear; the main refinements implemented on the test setup are discussed in section 4.7. Further, a discussion about how sources of error might have influenced the results is present in chapter 6.

In this experiment, efforts were made to reduce systematic errors by proper calibration of devices, controlled environmental conditions, and having a clear test procedure that is followed for every test. On the other hand, random errors, while can be reduced, are virtually impossible to eliminate. The main measures taken to minimise sources of random errors relevant to this work are listed below:

- Eccentricity between the upper and lower rings was controlled using steel angles. Additionally, geometry scans are done for several test assemblies to validate the accuracy of the steel angles (refer to Section 4.7 for more details).

- Off-centered placement of glass specimens was minimized by aligning the center lines marked on the specimen's surface during preparation with the center lines of the lower plate.
- The verticality of the displacement sensor was maintained using a water level device. The same procedure was replicated for all test specimens to minimize measurement error.
- The magnitude of the tightening of the bolts connecting the upper and lower rings was controlled by placing markers on each bolt to indicate a standard magnitude that is followed in every test.
- The installation of strain gauges was done according to a fixed set of sequential procedures that are followed for every test to minimize human error.

4.7 Challenges and adaptations in the experimental setup

Unpredictability comes hand in hand with experimental testing, especially if the testing method is novel or there is limited literature about it. Plenty of unforeseen challenges have been encountered during the process of developing this test setup as functioning and reliable, which led to considerable delays compared to the initial timeline of progress. Pointing out and addressing issues in the test setup is considered one of the main contributions of this work. The main practical challenges faced during this experimental work are discussed below.

Challenge 1: Ejection of the rubber ring placed between the lower steel ring and the glass.

Description: because the rubber ring was only secured in place by means of friction, it could not hold its place against high water pressures, causing it to be explosively evicted from its position, as shown in Figure 4.9. This allowed water leakage and invalidated the test.

Adaptation: wider rubber ring with an inner diameter of 915 mm and an outer diameter of 585 mm was used instead of the narrower ring used initially. An attempt was made to glue the rubber to the steel ring using ethyl cyanoacrylate, but that was not enough to secure it in place under high water pressures. Ultimately, the idea of screwing the rubber ring to the lower steel plate arose as a practical and effective solution (see Figure 4.10). This tactic successfully maintained the lower rubber ring in place during testing.



Figure 4.9 Displaced rubber ring due to high water pressure.

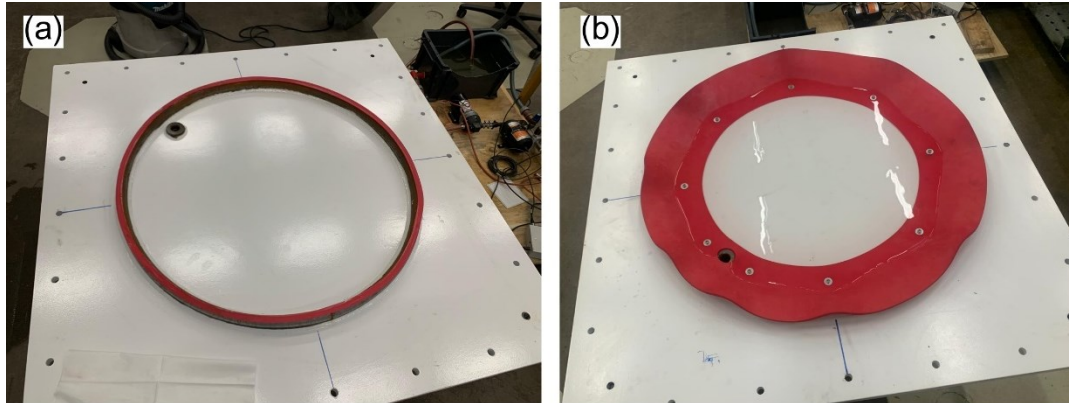


Figure 4.10 Method of securing the lower rubber ring in place: (a) rubber profile used initially; (b) rubber ring screwed to the lower steel plate.

Challenge 2: Stress concentration along the contact circle.

Description: the ideal stress state in the glass specimen is uniform, biaxial flexural stresses within the circle bounded by the steel rings, diminishing towards the edges. Areas of stress concentration are undesirable and can cause ring failures, rendering a test invalid. Stress concentration can happen due to several causes. Excessive compression exerted by the steel rings on the glass (due to tightening), boundary conditions where in-plane movement is totally restricted, and misalignment between the upper and lower rings that can generate internal bending moment in the glass are some of the main driving factors of stress concentration.

Adaptation: since the issue of stress concentration involves multiple factors, it is addressed through a series of adjustments to the test setup rather than a single solution. The main adjustments implemented to tackle this challenge are:

- Changing the type of lubricant applied between the rubber ring and the glass from Polytetrafluoroethylene (Teflon oil), which is recommended by the ASTM 1499-8 standard [53], to petroleum jelly, which proved more efficient.
- Marking the bolts connecting the upper and lower rings as a gauge for the desired amount of tightening, as excessive tightening results in stress concentration and insufficient tightening results in water leakage.
- Using two rubber rings instead of one, each with a different hardness, in between the steel rings and the glass. Linatex rubber (red color) with a shore A hardness of 38 and thickness of 5 mm is placed in contact with the glass, while Neoprene rubber with a shore A hardness of 50 and thickness of 3 mm is in contact with the steel ring.

Challenge 3: water leakage.

Description: as water is pressurized to high pressures, up to 2.4 bar, leakage is a major issue as it would result in a pressure drop. Water leakage primarily happened due to insufficient or unstable sealing. Nonlinear pressure buildup or sudden spikes in pressure is also a contributing factor to water leakage. During the initial tests, the system could only reach pressures around 1.4 bar before leaking starts to happen.

Adaptation: at first, a sealant material (Sikasil WS-605) was applied along the lower steel ring. However, while this approach slightly improved the sealing properties of the test setup, it was not sufficient to reach the desired pressure without leakage. It then became apparent that a combination of proper tightening, where the bolts connecting the two rings are tightened to an ideal point that is tight enough to prevent leaking but not overly tight to cause intense stress concentration, and the tuning of the PID controller to maintain a linear pressure buildup and eliminate any sudden rise of pressure in an effective strategy to reach the desired pressures without leakage. Also, as mentioned before, the use of a wide rubber ring that is secured in place favorably improved the sealing and prevented water leakage.

Challenge 4: excessive eccentricity between the upper and the lower ring.

Description: eccentricity between the two rings can cause internal bending moment within the glass plate at the area of contact, which can cause undesired failure; Figure 4.11 presents a visual illustration of this behaviour. The upper and lower rings are identical in shape and dimensions, as it was verified by geometric scanning. Therefore, measuring eccentricity is done through measuring the horizontal offset between the edges of the plates. Through practice, it was deemed that an acceptable limit of eccentricity is 2 mm.

Adaptation: a proposal of using metal rods to maintain concentricity was adopted at first. That is, since the upper and lower steel plates have the same shape and dimensions, connecting their four corners with low-tolerance vertical metal rods that go through holes in both plates seemed like an effective

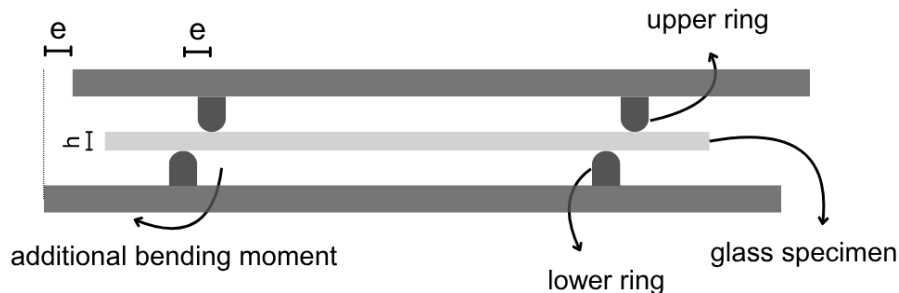


Figure 4.11 Schematic representation of a cross-section of the test setup, showing the effect of eccentricity (e).

solution by intuition. However, the idea proved inefficient due to imperfect flatness of the steel rings at the edges. Thus, metal steel angles were used to maintain concentricity by vertically aligning the four edges of the two plates. In addition, geometry scans were performed on the test setup before testing as a method of verification to ensure the eccentricity does not exceed the allowable limit. The scans are done using Atos Compact Scan 3D scanner, and the data analysis is performed using the accompanying software named GOM Inspect. The geometric scan of one of the tests is presented in Figure 4.12, where the edge of the upper plate is used as reference vertical plan and the horizontal deviation of the lower plate is indicated in mm.

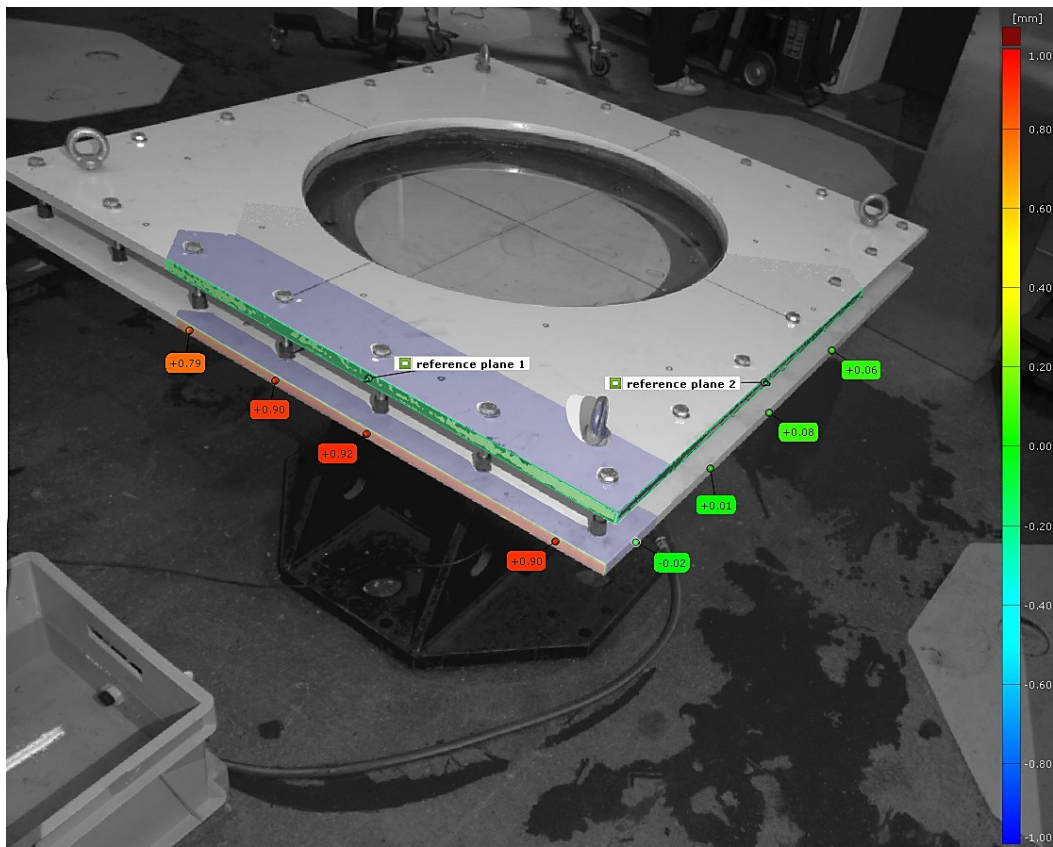


Figure 4.12 Geometry scan of the test setup, showing the misalignment between the upper and lower plates.

5 Results

The relevant results and findings are presented in this section. A certain number of tests were considered invalid either due to improper failure origin location or inconsistent behaviour compared to the general pattern exhibited by the majority of the specimens. The data from these invalid tests still, however, considered valuable to build an understanding of the influencing factors on the test setup. The load and deflection data are recorded for every test, while strain data and DIC data are only available for few tests. Each specimen is designated a unique identifier from 1 to 21, consecutively. The specimen identifier also serves as the test number, indicating the chronological order of testing. Table 5.1 presents an overview of the status of the tests, showing the radial distance from the center of the specimen to the failure origin. Out of the 21 tests conducted, 13 tests are considered valid, while 8 are invalid.

Table 5.1 Overview of the status of the tests showing the radial distance from the failure origin to the center of the specimen for each test.

Test number	Status	Notes	Radial distance (mm)
1	Invalid	Ring failure	400
2	Valid	—	202
3	Invalid	Ring failure	400
4	Valid	—	235
5	Valid	—	234
6	Valid	—	116
7	Invalid	Ring failure	400
8	Invalid	Ring failure	400
9	Invalid	Inconsistent behaviour	107
10	Invalid	Inconsistent behaviour	114
11	Valid	—	201
12	Valid	—	192
13	Valid	—	29
14	Valid	—	115
15	Valid	—	34
16	Valid	—	158
17	Valid	—	192
18	Valid	—	219
19	Invalid	Ring failure	400
20	Valid	—	206
21	Invalid	Ring failure	400

5.1 Time history response

To provide an overview of the testing process, time histories of the load and deflection are presented. Load refers to the uniform pressure acting on the specimen's circular area bounded by the upper and lower rings, while deflection refers to the central displacement exhibited by the specimen as it is loaded. Since the time history response for all specimens is very similar, it is presented only for an example specimen (specimen 14). Figure 5.1 shows the load vs time as well as the deflection vs time relationship for that specimen. As shown in the figure, the response is divided into two phases. The first phase can be referred to as a pre-loading phase, as its main purpose is to stabilize PID controller, after which the actual loading phase begins (refer to section 4.3 for more details). During the loading phase, the load increases approximately linearly until the specimen fails, while the corresponding deflection increases nonlinearly with respect to the load.

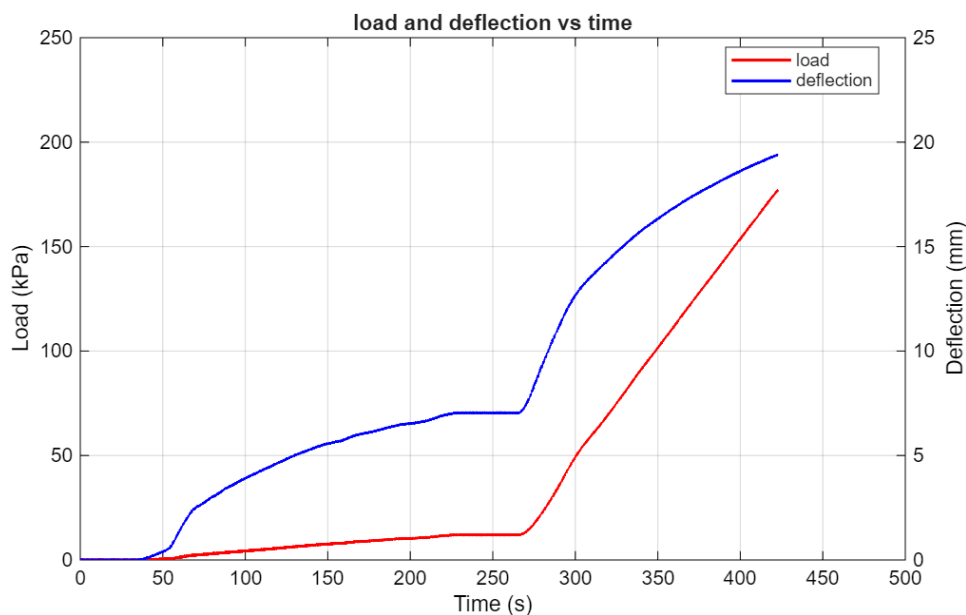


Figure 5.1 Time history response for load and deflection.

5.2 Load-deflection relationship

The load-deflection relationship for all 21 performed tests is presented in Figure 5.2, where deflection is in mm and pressure is in kPa, with vertical lines indicating the failure pressure for each specimen. The strength variability discussed in Chapter 3 manifests itself clearly in the Figure. The relationship between load and deflection is a nonlinear curve, where the specimen shows a softer behaviour initially, followed by a gradual stiffening as the load increases. As it is clear in Figure 5.2, there is a general pattern followed for the majority of the tests where most curves are condensed. Significant deviation

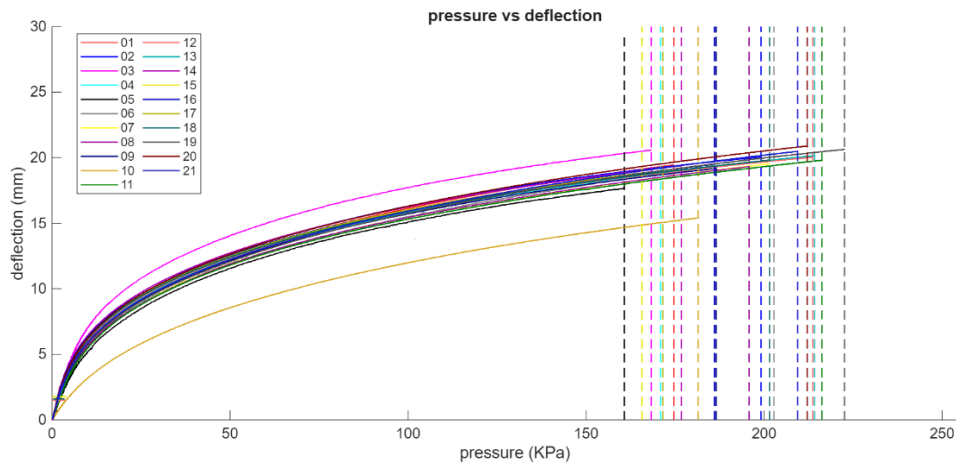


Figure 5.2 Load-deflection curve for all specimens.

from that pattern, as in specimen 10, would render a test invalid, as it potentially marks a procedural mistake that went unnoticed. To make an objective measure of what is considered too much deviation from the average, the mean value of the deflection at a specific load point of 160 kPa is calculated, and specimens that show a variation beyond 5% of the mean are discarded. The fixed load point was chosen as the highest load that is common to all specimens. Based on that approach, the mean is calculated as 18.3 mm, and specimens with deflection values outside the range of 17.4 mm and 19.2 mm do not constitute a valid test. For specimen 9, although it follows that general pattern, the test is considered invalid because there has been a water leakage during the test. This resulted in the test being halted midway before failure to unload the specimen and lower the pressure, then load it again, which might have altered the standard test conditions somehow, since the specimen failed at a lower load compared to what it has already reached during the first loading. It can also be observed that most of the curves of the specimens that had a ring failure follow the general pattern, but because these specimens did not fail due to a uniform flexural stress, they are considered invalid tests. Figure 5.3 shows the load-deflection curves of only the valid tests.

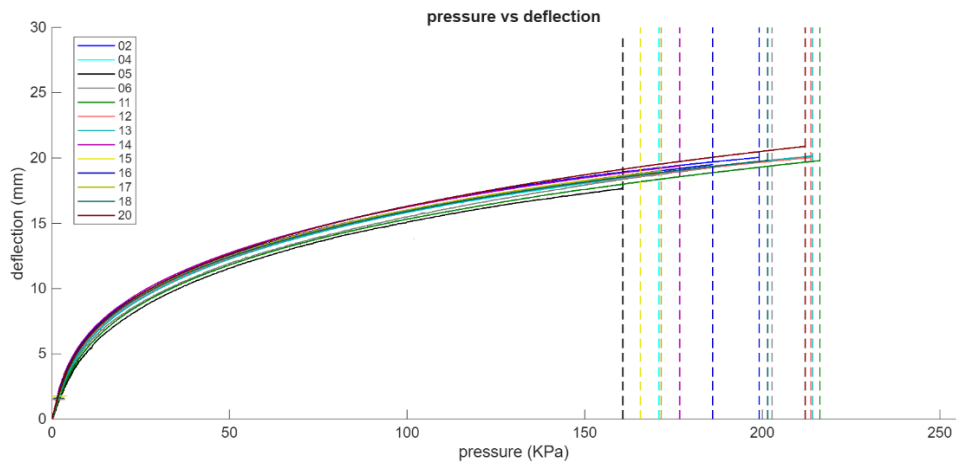


Figure 5.3 Load-deflection curve for valid specimens only.

5.3 Strain gauges results

Strain data are available for specimen 6 and specimen 21. Strain data at two different locations (see Figure 4.5) are recorded for each specimen. As explained in section 4.4, strain is measured along three different directions; these strain components are then used to calculate the principal stress. The relationship between the load and the strain, in each of the three directions, for specimens 6 and 21 is presented in Figure 5.4. For both of the specimens, the two strain gauges show remarkably similar results, which suggests that the strain within the specimen, and in turn the stress, is somewhat uniform for the points having the same radial distance from the center. Moreover, it can be seen that the strain in the radial direction (b channel) is maximum compared to the other two channels which are parallel to the X- and Y-axis of the specimen; this behavior aligns with the theoretical expectations for the glass mechanical behavior, assuming a thin plate model.

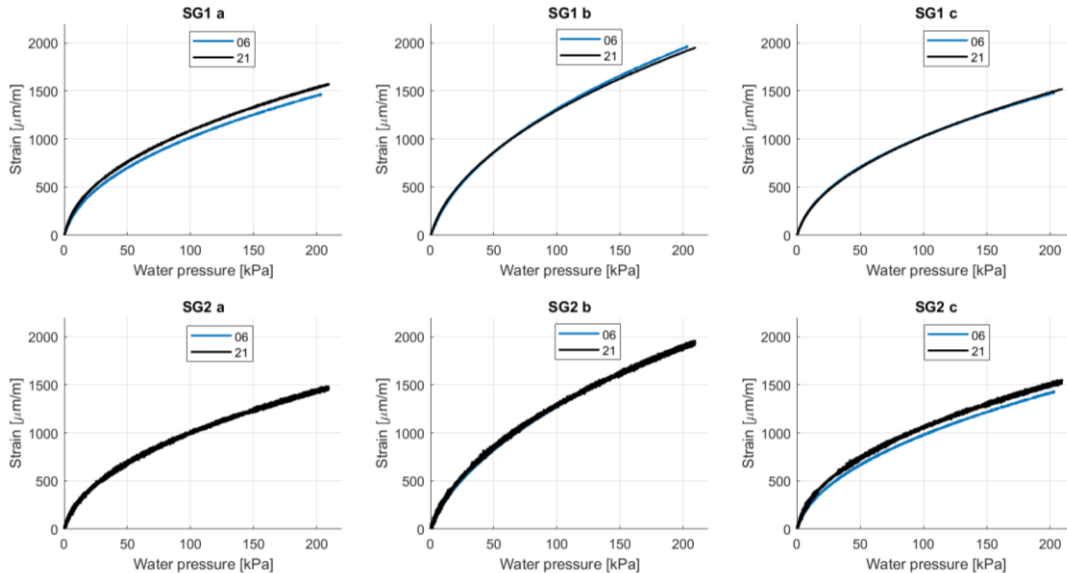


Figure 5.4 Strain results for specimen 6 and specimen 21.

Eq. 5.1a is used to calculate the major principal stress at the location of the strain gauges, with $E = 70000 \text{ MPa}$ and $\nu = 0.23$. The relationship between the load and the major principal stress at the locations of the strain gauges is presented in Figure 5.5. Both specimens showed highly similar stress results at the two locations where the strain was measured. Notably, the two specimens failed at a very similar pressure of 2 bar and 2.1 bar for specimen 6 and specimen 8, respectively. This is reflected in Figure 5.5 as specimen 21 sustained slightly higher pressure than specimen 6. Further, the failure origin of specimen 6 was only 110 mm away from the location of strain gauge 1 (SG1), while specimen 21 failed at the contact ring.

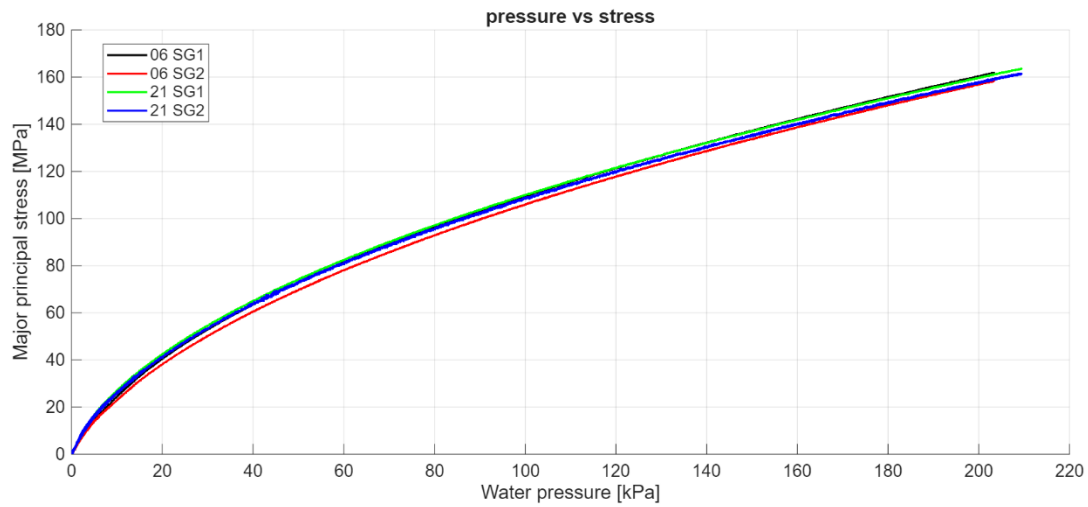


Figure 5.5 Relationship between load in kPa and the major principal stress in MPa for specimen 6 and specimen 21.

5.4 DIC results

DIC was utilized for specimens 12, 13, and 21, with a different type of speckle pattern being used for specimen 21 (refer to section 4.4 for more details). Since DIC results can contain loads of output data, only the most relevant to the scope of this work is presented in this section. The main output data from the DIC include the out-of-plane displacement field, the in-plane strain field, and the major principal stress field. All the presented DIC results are for the last frame before failure, where the stresses and strains are maximum, unless otherwise stated. The vertical displacement field of the three specimens is almost identical, and therefore it will only be presented for specimen 12 to avoid repetition. Moreover, some parts along the specimen surface might be interrupted by physical obstacles (e.g., displacement sensor) or affected by poor speckle pattern quality (e.g., along the edges); those areas are eliminated from the results.

Specimen 12:

Vertical displacement:

The vertical displacement of the specimen is shown in Figure 5.6. The displacement field is continuous, peaking at the central area with around 26 mm. It can be observed that there is some vertical rigid body motion happening within the test setup where the entire upper steel plate moves. In turn, the beam on which the displacement sensor is mounted moves as well, which leads to the central deflection not being consistent with the displacement sensor data from Figure 5.3. Therefore, the DIC measurement is absolute where the displacement sensor measurement is relative to the whole setup.

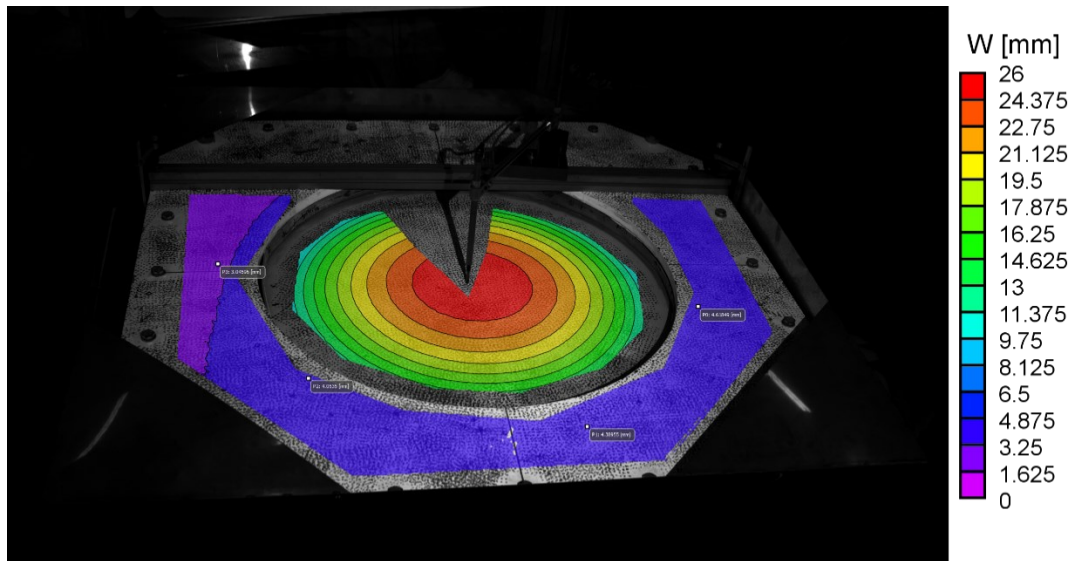


Figure 5.6 Vertical displacement field of specimen 12.

Principal strain:

The maximum in-plan strain field is shown in Figure 5.7. The Figure shows that the strain is relatively uniform within the specimen's surface, ranging between 0.17% and 0.2%.

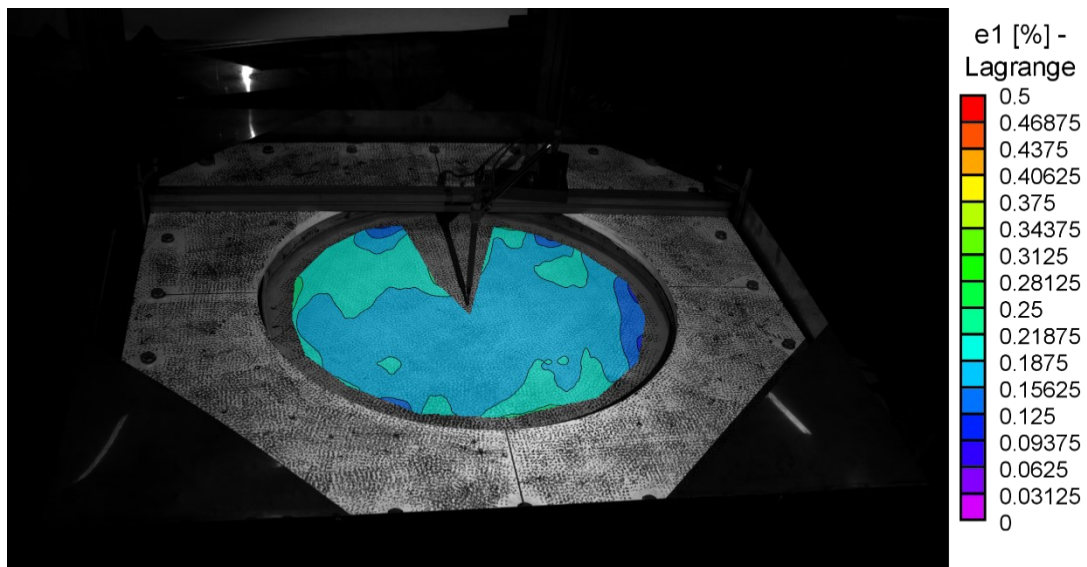


Figure 5.7 Principal strain field of specimen 12 just before failure.

Principal stress:

The principal stress is directly calculated by defining glass as a material model. Since glass is a linear elastic material, a uniform strain field directly translates into a uniform stress field, as shown in Figure 5.8. The stress ranges between 140 MPa and 180 MPa.

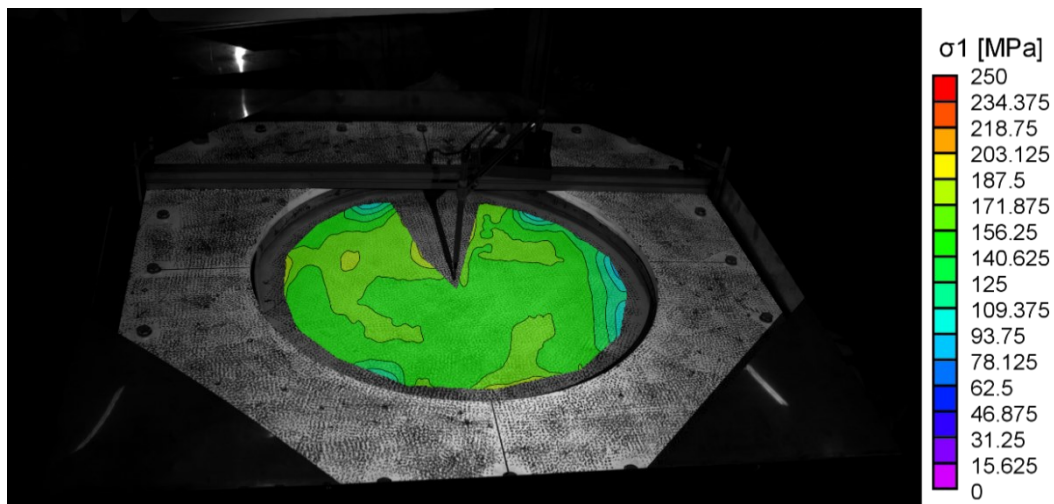


Figure 5.8 Principal stress field of specimen 12 just before failure.

Specimen 13:

Principal strain:

The principal strain field is presented in Figure 5.9. The specimen is undergoing less strain compared to specimen 12. The strain field, however, is still considered relatively uniform, ranging from 0.12% to 0.18%.

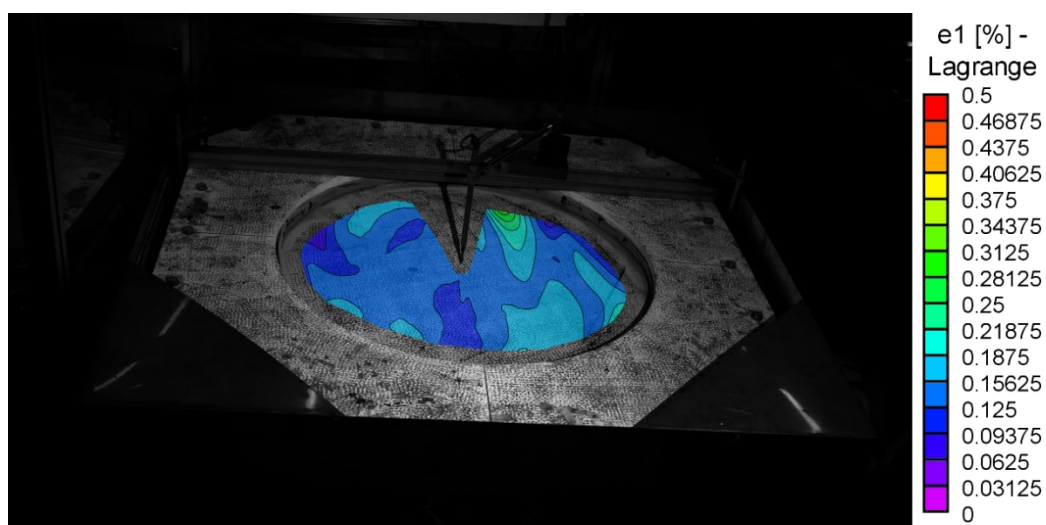


Figure 5.9 Principal strain field of specimen 13 just before failure.

Principal stress:

Figure 5.10 shows the principal stress field. For most of the specimen's surface, the stress ranges between 120 MPa and 150 MPa, with one location showing significant stress concentration near the contact ring. The localised stress, however, was not high enough to cause a ring failure.

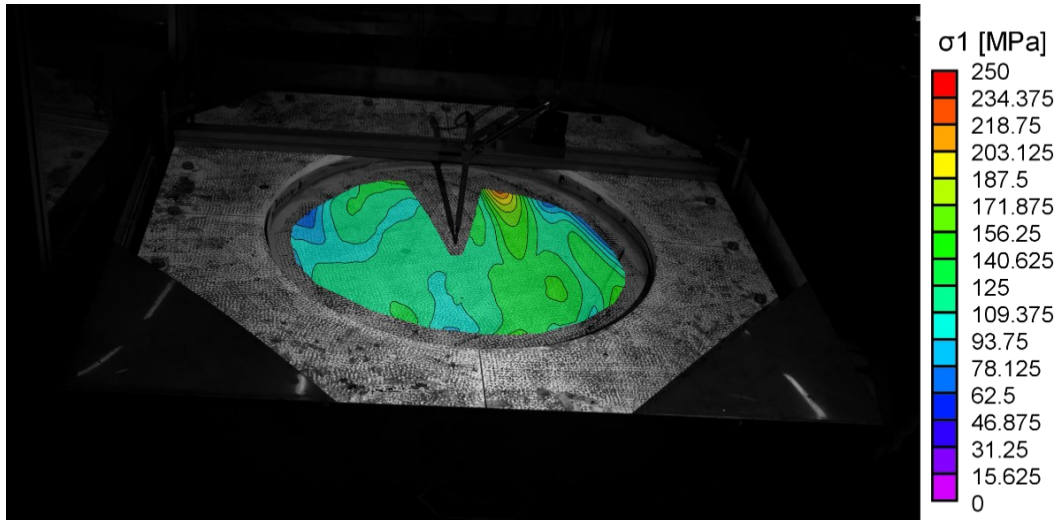


Figure 5.10 Principal stress field of specimen 13 just before failure.

Specimen 21

Initial condition:

Deliberate change to the orientation of the upper plate was made by rotating it 90° compared to the typical orientation to assess the influence on alignment. Figure 5.11 presents the out-of-plane special coordinates of the specimen before starting the test. The Figure reveals that the change in the plate's orientation led to significant deformations between -1 mm and $+0.6$ mm in the pre-testing condition compared to about ± 0.2 mm for specimens 12 and 13. As discussed in section 4.7, this misalignment could result in pre-stressing the specimen, leading to a nonuniform stress field during testing and, potentially, areas of stress concentration.

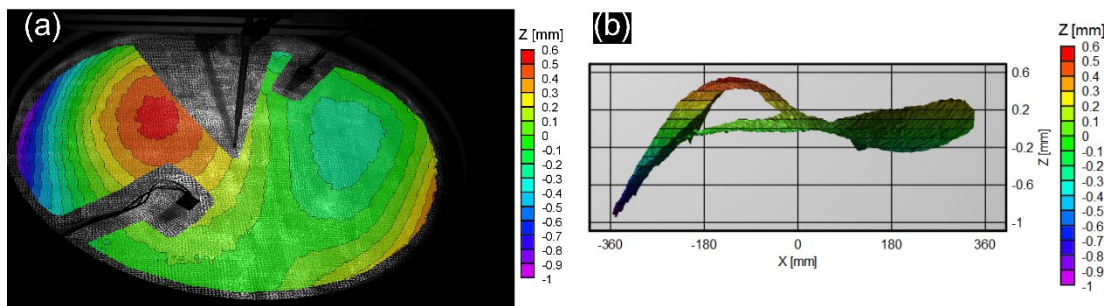


Figure 5.11 Out-of-plane spatial coordinates of the specimen surface in the pre-testing state: (a) 2D contour; (b) scaled side profile of the 3D contour.

Principal strain:

The principal strain field of the specimen is presented in Figure 5.12. The strain is less uniform compared to specimens 12 and 13. One region is seen to have extremely high strain.

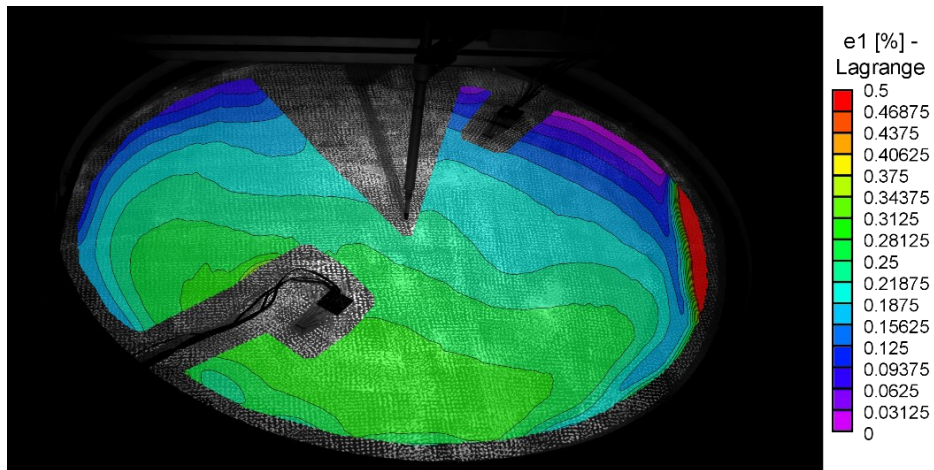


Figure 5.12 Principal strain field of specimen 21 just before failure.

Principal stress:

As the principal stress is directly related to the principal strain, a non-uniform stress field is expected to occur within the specimen, as shown in Figure 5.13. The stress gradient is continuous, transitioning from a relatively high stress area of about 220 MPa to diminish gradually as it reaches the edges. A significant stress concentration can be seen on one spot along the contact ring; this spot marks the location of the failure origin. This stress nonuniformity and the intense stress concentration are likely caused by the misalignment between the two rings.

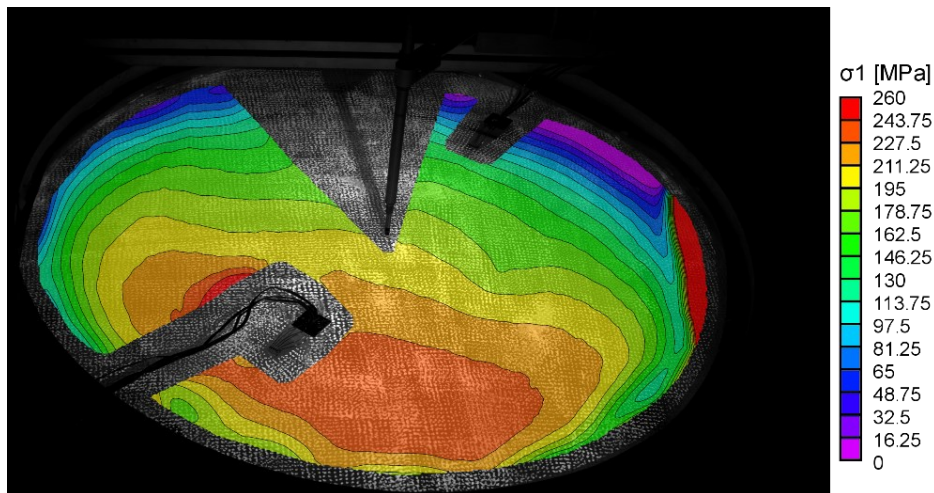


Figure 5.13 Principal stress field of specimen 21 just before failure.

Comparison between strain gauges and DIC:

Since both strain gauges and DIC were used in this test, a comparison between their results is possible. The major principal stress will be used as the comparison variable. Nonetheless, the comparison is essentially restricted by the fact that the DIC cannot measure any data at the locations occupied by strain gauges; therefore, an interpolation of values around those locations is

necessary to infer the stress results at the desired spots. It should be noted that the DIC measures full-field strains. In contrast, strain gauges measure strain over an extremely small area; thus, perfect consistency is not expected, but rather a reasonable agreement between the results. Moreover, previously presented DIC strain results were calculated using a moderately large filter size of 50 to smooth out the results and eliminate unnecessary noise. Some details, however, might be lost with such a high filter size, and therefore a lower filter size of 20 is used for this comparison for a more accurate strain calculation over smaller areas. That said, Figure 5.14 presents the principal stress results from the DIC around the locations of the two strain gauges, with inspection points showing the stress values at different spots. This is the stress in the frame just before failure; the corresponding stress calculated through strain gauges is 163 MPa and 161 MPa for SG1 and SG2, respectively (refer to Figure 5.5). The DIC results show that the stress around SG1 ranges between 157 MPa and 135 MPa, which is reasonably consistent with SG1 results, yet it shows a considerably higher stress ranging from 182 MPa to 225 MPa around SG2. It is not possible to deduce the stress at the location of the strain gauge, as the stress around it is considerably nonuniform, but the surrounding stress values are highly suggestive that there is an inconsistency with the strain gauge.

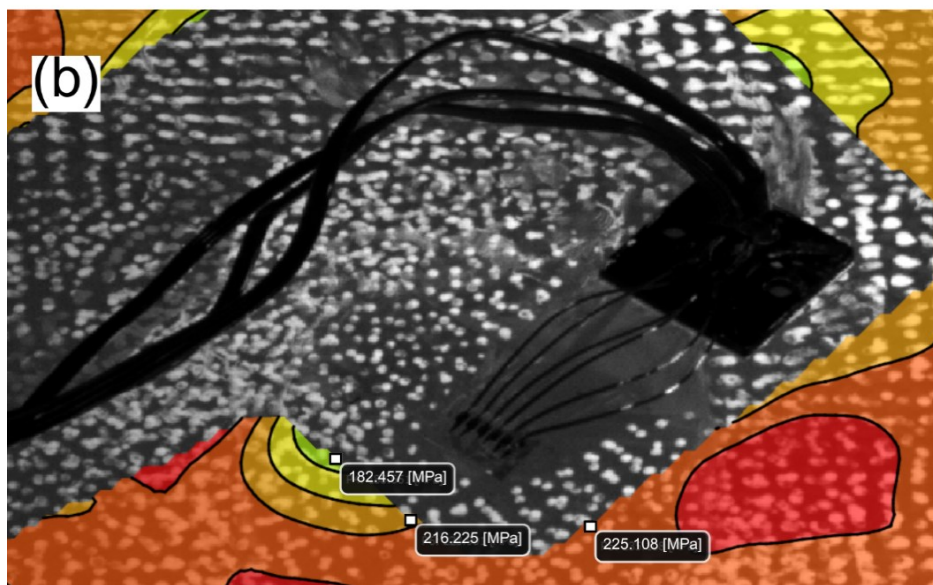
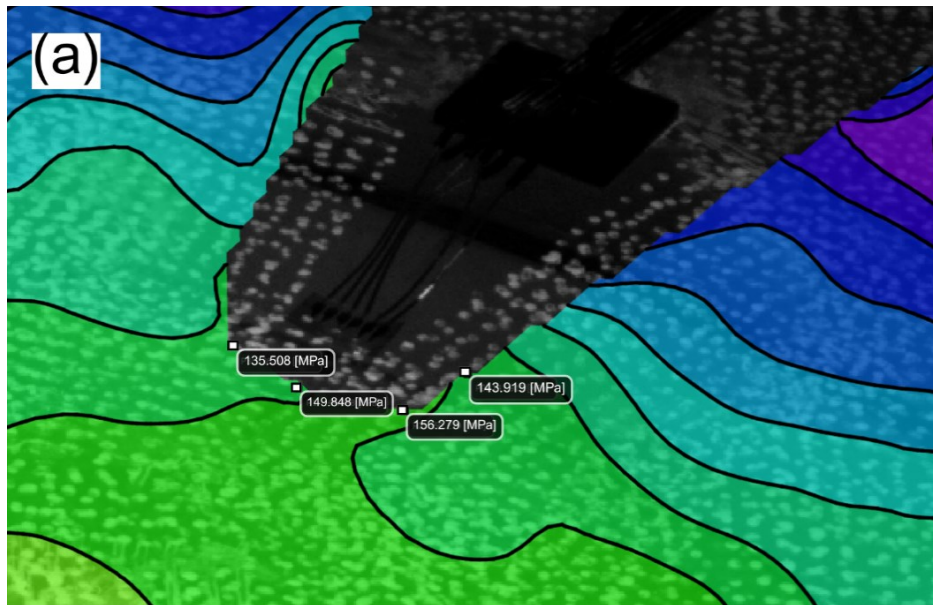


Figure 5.14 Principal stress results from DIC near the location of strain gauges: (a) SG1; (b) SG2.

6 Discussion and conclusions

6.1 Main findings

This research aimed to propose a novel testing technique for glass strength utilizing the CDR method to offer a simpler, more efficient alternative to the current standard testing methods. After a continuous process of iterative refinement of the test setup, 21 specimens with identical nominal dimensions were tested, out of which 13 are considered valid, where the majority of the invalid tests occurred during the early stages of testing.

The valid specimens demonstrated a consistent pattern in terms of the load-deflection relationship. The average maximum deflection was about 20 mm. For all specimens, the deflection rate with respect to load was significantly higher during the early stages of loading, then it gradually declines as the deflection increases. This behaviour marks the emergence of the membrane effect discussed in section 3.4, indicating that the specimens are well into the geometrically nonlinear region. There was a considerable strength variation between the specimens, ranging from 160 kPa to 220 kPa. This is due to the inherent surface flaws existing in the glass, which largely control its strength. Given a large enough dataset, the strength values could potentially be analysed using a suitable statistical model to arrive at a characteristic strength, but this lies outside the scope of this work.

Strain gauges were used in two different tests, and their results showed highly consistent strain and, in turn, highly consistent stress in two different locations along the specimens' surface; not only that, but the strain results from the two specimens were very close to each other. Furthermore, DIC results from two different specimens showed that the stress field along the surface is uniform to a great degree. The maximum stress calculated through strain gauges was around 163 MPa, while DIC images showed a stress range of around 120 MPa to 180 MPa in the frame just before failure. These results are somewhat consistent with the strength values for tempered glass available in the literature.

For one specimen, however, the stress field was non-uniform, where there was a localised region of higher stress that diminished towards the edges. This specimen also showed an area of significant stress concentration that ultimately led to its failure. For this same specimen, a comparison between strain gauges and DIC was possible as both were utilized, although highly compromised since the locations of the strain gauges are excluded from the DIC results. In terms of major principal stress, one strain gauge (SG1) showed good agreement with the DIC results, while the other strain gauge (SG2) was potentially inconsistent with the DIC. The reason behind this inconsistency is not exactly clear. It should be emphasized, however, that there

was an unusual misalignment in the test setup of this specimen due to an experimental change to the upper plate's orientation, which might have disturbed the uniformity of the stress field.

6.2 Discussion of results

Compared to the standardized CDR method, the proposed testing technique provides significant advantages with respect to simplicity of conducting the test, the uniformity of the stress field, as well as utilizing the stretching of the mid-surface as the primary load-carrying mechanism instead of bending. The results essentially extend the state of the art by demonstrating that maintaining a uniform stress field is viable while having large deflections, and thus presenting a more efficient alternative to the testing methods currently in use.

While the proposed test setup has undergone significant improvements during the process of its development, there could still be some minor refinements to be made to improve the consistency of the results. It should be noted, however, that occasional invalid tests (e.g., 1 in 10 tests) do not undermine the reliability of the test setup but are rather expected as a natural aspect of experimental testing.

Since all the specimens are virtually identical and are tested under similar test conditions, the results for all the specimens should ideally be aligned. However, the results showed that there is some degree of inconsistency between specimens in terms load-deflection relationship as well as the stress field created within the loaded area. This inconsistency can be attributed to several sources of random error that have potentially influenced the results, although the extent of this influence might not be fully clear. The main sources of error introduced in this experiment are listed below:

- Eccentricity between the lower and the upper ring – there exists an inevitable deviation from the ideal concentricity between the two rings, which could change in magnitude and direction for each test assembly, which could influence the stress field.
- Vertical misalignment of the displacement sensor – slight deviation from verticality, which varies in magnitude and direction, is expected each time. This error can result in a small underestimation of the true central deflection of the glass specimen.
- Uneven tightening of the bolts connecting the lower and upper rings – the magnitude of the tightening of the connecting bolts is not exactly the same for each test. Overly tight bolts can cause stress concentration along the contact region, while under-tightened bolts can cause water leakage at higher pressures.

- Differing amounts of lubricant between the glass and rubber – petroleum jelly (commonly known as Vaseline) is used as a lubricant. As the lubricant is applied manually, its amount can vary from test to test, which can affect the boundary conditions.
- Manual installation of strain gauges – misalignment of the strain gauge measuring grids with the specimen's axes and uneven adhesion between the strain gauge and the glass surface are potential random errors that can occur while installing strain gauges, which can affect the accuracy of the strain measurement.
- Non-uniform speckle pattern for DIC imaging – speckle pattern is applied manually using a roller and ink, which results in some areas being denser than others. This can affect the image resolution and strain measurement accuracy.

6.3 Conclusions and future work

Based on the results obtained from this work, the following conclusions can be drawn:

- The proposed test setup proved capable of reproducing the same boundary and loading conditions; this is indicated through the consistency of the load-deflection relationship among all the valid specimens.
- The location of the failure origin appeared to be random. That is, it did not show any preferential radial distance nor angle along the specimen's surface.
- The test setup underwent various refinements and modifications to improve its functionality. A big part of the efforts was directed towards reducing stress concentration along the contact circle to prevent undesired failures, and it seemed that modifying the boundary conditions to allow, to a certain degree, for horizontal movement was crucial for achieving this goal.
- The proposed testing technique is capable of creating a somewhat uniform stress field within the test area while having large deflections; as well, it is capable of producing a similar, repeatable stress field across different specimens. This can be seen from the principal stress results obtained from strain gauges, as well as the DIC images.
- Specimens develop geometrically nonlinear behaviour beyond a certain point. This is marked by a stiffening of the specimen where the rate of change of deflection with respect to load declines as the plate exhibits larger deflections. This indicates a transition of the load-

carrying mechanism of the plate from bending to stretching of the middle surface (membrane effect).

- The proposed test setup has the potential to offer a significant advantage over the current standard testing methods as it is simpler to perform, able to create a uniform stress field, and efficient in utilizing geometric nonlinearity.

To build upon the findings of this work, future research that includes a larger number of specimens is needed to further validate the test setup as well as enable a statistical evaluation of the data. For that, continuation of the experimental program is planned to happen with 29 more specimens, which will allow for statistically modelling the data and determining a characteristic strength value for tempered glass. Other future research that builds upon this work could include testing circular specimens to investigate the influence of the specimen's shape on the results. Besides, a comparison with numerical simulation, where geometric nonlinearity is considered, could provide valuable information for further validation of the experimental findings, as well as for evaluating the influence of different parameters (e.g., specimen's thickness, radius of the rings, etc.) on the mechanical response of glass.

References

- [1] Shelby JE. Introduction to Glass Science and Technology. Royal Society of Chemistry;2020.
- [2] Angelini I, Gratuze B, Artioli G. Glass and other vitreous materials through history. Mineralogical Society of Great Britain and Ireland eBooks [Internet]. 2019;87–150.
- [3] Veer F, Louter P, Bos F. The strength of annealed, heat-strengthened, and fully tempered float glass. *Fatigue and Fracture of Engineering Materials and Structures*. 2009 Jan;32(1):18–25.
- [4] Veer F. The strength of glass, a nontransparent value. *Heron*. 2007 Jan 1;52:87–104.
- [5] Heiskari J, Romanoff J, Laakso A, Ringsberg JW. On the lightweight design of laminated insulating glass units in cruise ships. *Ships and Offshore Structures*. 2024 Sep 13;1–19.
- [6] Wurm J. *Glass structures: design and construction of self-supporting skins*. Basel: Boston; 2007.
- [7] Pisano G. The statistical characterization of glass strength: from the micro- to the macro-mechanical response [Thesis]. Università degli Studi di Parma; 2017.
- [8] European Committee for Standardization (CEN). EN 1288-1. Glass in building - Determination of the bending strength of glass - Part 1: Fundamentals of testing glass. Brussels, Belgium: 2000.
- [9] Meyland MJ, Nielsen JH, Kocer C. Tensile behaviour of soda-lime-silica glass and the significance of load duration – A literature review. *Journal of Building Engineering*. 2021 Dec 1;44:102966.
- [10] Castori G, Speranzini E. Fracture strength prediction of float glass: The Coaxial Double Ring test method. *Construction and Building Materials*. 2019 Nov;225:1064–76.
- [11] Dall'Igna R, D'Este R, Mirko S. Comments on test methods for determination of structural glass strength. *Proceedings XXV ATIV Conference*. 2010;5–13.
- [12] Pisano G, Carfagni CR. Towards a new standardized configuration for the coaxial double test for float glass. *Engineering Structures*. 2016;119:149–63.
- [13] Ventsel E, Krauthammer T. *Thin Plates and Shells: Theory, Analysis, and Applications*. CRC Press; 2001.
- [14] Varshneya AK, Mauro JC. *Fundamentals of Inorganic Glasses*. Elsevier; 2019.

- [15] Bourhis E. Glass: mechanics and technology. Weinheim: Wiley-VCH; 2014.
- [16] Uusitalo O. Float Glass Innovation in the Flat Glass Industry. Springer International Publishing; 2014.
- [17] Haldimann M. Fracture strength of structural glass elements – analytical and numerical modelling, testing and design [Thesis]. École Polytechnique Fédérale de Lausanne; 2006.
- [18] Adams LH, Williamson ED. The annealing of glass. Journal of The Franklin Institute - Engineering and Applied Mathematics. 1920 Nov 1;190(5):597–631.
- [19] Acloque P. Verres Refractaires. 1951;5:247.
- [20] Nielsen JH, Olesen JF, Poulsen PN, Stang H. Finite element implementation of a glass tempering model in three dimensions. Computers and Structures. 2010 Sep;88(17–18):963–72.
- [21] Erdem İ, Guldiren D, Aydin S. Chemical tempering of soda lime silicate glasses by ion exchange process for the improvement of surface and bulk mechanical strength. Journal of Non-Crystalline Solids. 2017 Oct 1;473:170–8.
- [22] Sun H, Dugnani R. Precise residual stress profile in ion-exchanged silicate glass by modified contour method. Journal of the European Ceramic Society. 2021 Feb 23;41(7):4355–68.
- [23] Leboeuf V, Blondeau JP, De Sousa Meneses D, Véron O. Potassium ionic exchange in glasses for mechanical property improvement. Journal of Non-Crystalline Solids. 2013 Oct;377:60–5.
- [24] GLASS [Internet]. architecture-history.org. Available from: <http://architecture-history.org/schools/GLASS.html>
- [25] Morales-Bravo J, Navarrete-Hernandez P. Enlightening wellbeing in the home: The impact of natural light design on perceived happiness and sadness in residential spaces. Building and Environment. 2022 Aug 8;223:109317.
- [26] Arbab M, Finley JJ. Glass in Architecture. International Journal of Applied Glass Science. 2010 Mar;1(1):118–29.
- [27] Nur-E-Alam M, Vasiliev M, Yap BK, Islam MA, Fouad Y, Tiong Sieh Kiong. Design, fabrication, and physical properties analysis of laminated Low-E coated glass for retrofit window solutions. Energy and Buildings. 2024 Sep 1;318:114427.
- [28] Patterson M. Structural glass façades and enclosures. Hoboken, N.J.: Wiley; 2011.
- [29] Meyer Turku | Exceptional quality since 1737 [Internet]. MEYER TURKU. 2024. Available from: <https://www.meyerturku.fi/en/index.jsp>
- [30] Bureau Veritas. Rules for the Classification of Steel Ships; PART B – Hull and Stability. 2019.

- [31] Lloyd's Register. Rules and Regulations for the Classification of Ships (LR-RU-00). 2024.
- [32] Station Eindhoven Centraal - bureauEAU [Internet]. bureauEAU. 2024. Available from: <https://www.bureaueau.nl/projecten/station-eindhoven-centraal-bureau-eau/>
- [33] Fotia F. Cina: lo spettacolare ponte di vetro sul Grand Canyon [GALLERY] [Internet]. MeteoWeb. 2016. Available from: <https://www.meteoweb.eu/2016/06/cina-lo-spettacolare-ponte-vetro-sul-grand-canyon-gallery/707307/>
- [34] Glass in Building. Basic soda-lime silicate glass products. Part 1: Definitions and general physical and mechanical properties. Brussels, Belgium: 2016.
- [35] Orowan E. Rapture of plastic crystals. International Conference of Physics. London; 1934. p. 81–92.
- [36] Fernández-Posada C, Barron A. Analysis of commercial glasses with different strengthening treatments: Emphasis on the tin side, defects, structure connectivity and cracking behavior. *Journal of Non-Crystalline Solids*. 2019 May 15;518:1–9.
- [37] Inglis C. Stresses in a plate due to the presence of cracks and sharp corners. In: *Proceedings of the Institution of Naval Architects*. 1913;55:219–241.
- [38] Griffith A. The phenomena of rupture and flow in solids. *Philosophical Transactions of the Royal Society of London Series A*. 1921 Jan;221(582–593):163–98.
- [39] Irwin G. Analysis of Stresses and Strains Near the End of a Crack Traversing a Plate. *Journal of Applied Mechanics*. 1957 Sep 1;24(3):361–4.
- [40] Porter M. Aspects of Structural Design with Glass [Thesis]. The University of Oxford; 2001.
- [41] Mencik J. Strength and fracture of glass and ceramics. *Glass Science and Technology*. 1992.
- [42] Evans A, Wiederhorn S. Proof testing of ceramic materials—an analytical basis for failure prediction. *International Journal of Fracture*. 1974;10(3):379–92.
- [43] European Committee for Standardization (CEN). Glass in building - Procedures for goodness of fit and confidence intervals for Weibull distributed glass strength data. Brussels, Belgium: 2016.
- [44] Weibull W. A statistical theory of the strength of materials. *Royale Institute of Technology (KTH)*. 1939.
- [45] Trustrum K, Jayatilaka ADS. On estimating the Weibull modulus for a brittle material. *Journal of Materials Science*. 1979 May;14(5):1080–4.
- [46] Datsiou KC, Overend M. Weibull parameter estimation and goodness-of-fit for glass strength data. *Structural Safety*. 2018 Jul 1;73:29–41.

[47] Demchyna B, Osadchuk T. Flexural strength of glass using Weibull statistical analysis. *Journal of Achievements in Materials and Manufacturing Engineering*. 2018 Apr 1;87(2):49–61.

[48] European Committee for Standardization (CEN). Determination of the bending strength of glass - Part 3: Test with specimen supported at two points (four point bending). Brussels, Belgium: 2000.

[49] European Committee for Standardization (CEN). Determination of the bending strength of glass - Part 2: Coaxial double ring test on flat specimens with large test surface areas. Brussels, Belgium: 2000.

[50] European Committee for Standardization (CEN). Determination of the bending strength of glass - Part 4: Coaxial double ring test on flat specimens with small test surface areas. Brussels, Belgium: 2000.

[51] Castori G, Speranzini E. Experimental and Numerical Investigation of the Bending Strength of Glass. *Conference on Architectural and Structural Applications of Glass*. 2016.

[52] Quinn G. *Fractography of Ceramics and Glasses*. National Institute of Standards and Technology; 2020.

[53] ASTM International. *Standard Test Method for Monotonic Equibiaxial Flexural Strength of Advanced Ceramics at Ambient Temperature*. Pennsylvania, United States: 2009.

Appendix A: List of Figures

Figure 1.1 Graphical overview of the thesis.	12
Figure 2.1 2D atomic network of silicone dioxide (SiO ₂): (a) crystalline form of SiO ₂ where long-term order exists; (b) glassy form of SiO ₂ that lacks any long-term order; (c) Na ₂ -modified glassy form of SiO ₂	14
Figure 2.2 The float process [16].	15
Figure 2.3 Thickness control of glass ribbon through rotating rollers [15].	16
Figure 2.4 Stress profile of thermally tempered glass.	17
Figure 2.5 Working mechanism of tempered glass [17].	17
Figure 2.6 Residual stress profile from chemical tempering [15].	18
Figure 2.7 Fracture pattern of different glass types: (a) annealed glass; (b) heat-strengthened glass; (c) fully tempered glass [17].	19
Figure 2.8 Building glass façade in Espoo, Finland.	20
Figure 2.9 Cruise ship with a big glass dome [29].	21
Figure 2.10 Glass structural beams in Eindhoven central railway station, The Netherlands [32].	21
Figure 2.11 Pedestrian bridge with glass deck in Zhangjiajie, China [33].	22
Figure 3.1 The three modes of crack propagation: (a) Mode I: opening; (b) Mode II: sliding; (c) Mode III: tearing [7].	24
Figure 3.2 Linearized two-parameter Weibull distribution of glass strength [46].	28
Figure 3.3 Four-point bending test; L _b = 200 ± 1 mm and L _s = 1000 ± 1 mm, as per the European standard EN 1288-3.	31
Figure 3.4 Coaxial double ring test: (a) test setup for specimens with a small test area; (b) test setup for specimens with a large test area.	32
Figure 4.1 Schematic of the test setup (dimensions in mm).	35
Figure 4.2 Test setup.	36
Figure 4.3 Test specimens	36
Figure 4.4 Tin side detection test: (a) tin side of the glass with a white background; (b) air side of the glass with no white background.	37
Figure 4.5 Test specimen showing the placement of strain gauges.	39
Figure 4.6 Speckle pattern applied on the specimen surface: (a) ink speckle; (b) fluorescent speckle.	40
Figure 4.7 Fracture pattern of glass: (a) radial fracture pattern; (b) fracture pattern associated with ring failures.	40
Figure 4.8 Crack propagation captured by the Phantom V2012 camera: (a) specimen before fracture; (b) first frame (crack initiation); (c) second frame of the crack propagation; (d) third frame of crack propagation; (e) fourth frame of crack propagation; (f) specimen in its post-fracture state.	42
Figure 4.9 Displaced rubber ring due to high water pressure.	43
Figure 4.10 Method of securing the lower rubber ring in place: (a) rubber profile used initially; (b) rubber ring screwed to the lower steel plate.	44
Figure 4.11 Schematic representation of a cross-section of the test setup, showing the effect of eccentricity (e).	45
Figure 4.12 Geometry scan of the test setup, showing the misalignment between the upper and lower plates.	46
Figure 5.1 Time history response for load and deflection.	48
Figure 5.2 Load-deflection curve for all specimens.	49

Figure 5.3 Load-deflection curve for valid specimens only.	49
Figure 5.4 Strain results for specimen 6 and specimen 21.	50
Figure 5.5 Relationship between load in kPa and the major principal stress in MPa for specimen 6 and specimen 21.	51
Figure 5.6 Vertical displacement field of specimen 12.	52
Figure 5.7 Principal strain field of specimen 12 just before failure.	52
Figure 5.8 Principal stress field of specimen 12 just before failure.	53
Figure 5.9 Principal strain field of specimen 13 just before failure.	53
Figure 5.10 Principal stress field of specimen 13 just before failure.	54
Figure 5.11 Out-of-plane spatial coordinates of the specimen surface in the pre-testing state: (a) 2D contour; (b) scaled side profile of the 3D contour.	54
Figure 5.12 Principal strain field of specimen 21 just before failure.	55
Figure 5.13 Principal stress field of specimen 21 just before failure.	55
Figure 5.14 Principal stress results from DIC near the location of strain gauges: (a) SG1; (b) SG2.	57

Appendix B: source code for the PID controller

This appendix presents the code implemented in Arduino IDE software to maintain a linear water pressure buildup through a PID controller. The code was developed by Mohammad Izadi and modified by the author of this thesis to suit the specific requirements of this application.

```
#include <PID_v1.h>

// Pin configuration
const int outputPin = 9;

// PID variables
double Setpoint = 0.0, CurrentSetpoint = 0.0, InitialSetpoint = 0.0, Input, Output;
double Kp = 1400, Ki = 800, Kd = 0;
PID myPID(&Input, &Output, &CurrentSetpoint, Kp, Ki, Kd, DIRECT);

// Timing variables
unsigned long previousPrintTime = 0;
unsigned long rampStartTime = 0;
unsigned long rampDuration = 220000; // Ramp duration in milliseconds

// Safety limits
const float pressureMax = 2.6; // Maximum safe pressure

void setup() {
  // Initialize serial communication
  Serial.begin(115200);

  // ConFigure output pin
  pinMode(outputPin, OUTPUT);
  digitalWrite(outputPin, LOW);
```

```

// Initialize PID
myPID.SetMode(AUTOMATIC);
myPID.SetOutputLimits(0, 255); // Constrain output to valid PWM range

// Print instructions for live tuning and setpoint adjustment
Serial.println("Live PID Tuning and Linear Ramp for Setpoint Adjustment:");
Serial.println("Enter new values in the format:");
Serial.println(" - 'Kp=x.x' to set proportional gain");
Serial.println(" - 'Ki=x.x' to set integral gain");
Serial.println(" - 'Kd=x.x' to set derivative gain");
Serial.println(" - 'P=x.x' to set a new target pressure (in bar) with a ramp.");
}

void loop() {
// Update CurrentSetpoint to ramp smoothly to Setpoint
updateRamp();

// Read pressure
Input = readP1();

// Safety check
if (Input > pressureMax) {
digitalWrite(outputPin, LOW);
Serial.println("Error: Pressure exceeded limit! Pump stopped.");
return;
}

// Compute PID output
myPID.Compute();

// Apply the PID output
analogWrite(outputPin, constrain(Output, 0, 255));
}

```

```

// Output pressure data periodically
unsigned long currentMillis = millis();
if (currentMillis - previousPrintTime >= 1) { // Adjust interval as needed
  previousPrintTime = currentMillis;
  Serial.print("t ");
  Serial.print(currentMillis);
  Serial.print("\tP ");
  Serial.print(Input, 3);
  Serial.print("\tSP ");
  Serial.print(Setpoint, 3);
  Serial.print("\tCSP ");
  Serial.print(CurrentSetpoint, 3);
  Serial.print("\tKp ");
  Serial.print(Kp);
  Serial.print("\tKi ");
  Serial.print(Ki);
  Serial.print("\tKd ");
  Serial.println(Kd);
}

// Check for new PID values or Setpoint from Serial Monitor
readNewValues();
}

float readP1() {
  unsigned long sum = 0;

  // Average over 100 samples for a stable reading
  for (int i = 0; i < 100; i++) {
    sum += analogRead(A2);
  }

  // Calculate voltage

```

```

float voltage = (float(sum) / 100) * (5.0 / 1023.0);

// Convert voltage to pressure (linear relationship)
float pressure = 4 * voltage - 2; // Bar
return (pressure >= 0 && pressure <= 5) ? pressure : 0; // Clamp invalid values
}

void readNewValues() {
  if (Serial.available()) {
    String input = Serial.readStringUntil('\n'); // Read input until newline character
    input.trim(); // Remove extra spaces or newlines

    // Check for Kp, Ki, Kd, or Setpoint input
    if (input.startsWith("Kp=")) {
      Kp = input.substring(3).toFloat();
      myPID.SetTunings(Kp, Ki, Kd);
    } else if (input.startsWith("Ki=")) {
      Ki = input.substring(3).toFloat();
      myPID.SetTunings(Kp, Ki, Kd);
    } else if (input.startsWith("Kd=")) {
      Kd = input.substring(3).toFloat();
      myPID.SetTunings(Kp, Ki, Kd);
    } else if (input.startsWith("P=")) { // Setpoint adjustment with ramp
      double newSetpoint = input.substring(2).toDouble();
      if (newSetpoint >= 0 && newSetpoint <= pressureMax) { // Validate range
        Setpoint = newSetpoint;
        InitialSetpoint = CurrentSetpoint; // Save current setpoint as the initial setpoint
        rampStartTime = millis(); // Reset ramp start time
      } else {
        Serial.println("Invalid Setpoint. Must be between 0 and max pressure.");
      }
    } else {
      Serial.println("Invalid input. Use 'Kp=x.x', 'Ki=x.x', 'Kd=x.x', or 'P=x.x'");
    }
  }
}

```

```
    }  
  }  
}
```

```
void updateRamp() {  
  if (CurrentSetpoint != Setpoint) {  
    unsigned long elapsedTime = millis() - rampStartTime;  
  
    if (elapsedTime >= rampDuration) {  
      CurrentSetpoint = Setpoint; // Ramp complete  
    } else {  
      // Direct linear interpolation formula  
      double rampProgress = double(elapsedTime) / rampDuration;  
      CurrentSetpoint = InitialSetpoint + rampProgress * (Setpoint - InitialSetpoint);  
    }  
  }  
}
```
